

宇宙初期の超新星爆発時におけるダストの供給

野沢 貴也

北海道大学 大学院理学研究院 宇宙理学専攻

小笹 隆司、羽部 朝男(北大)、Eli Dwek(NASA)

梅田 秀之(東大)、富永 望(NAOJ)

前田 啓一(IPMU)、野本 憲一(東大/IPMU)

Contents

1. Introduction

2. Dust formation in the ejecta of Pop III SNe

(Nozawa et al. 2003, ApJ, 598, 785)

3. Dust evolution in Pop III SN remnants

(Nozawa et al. 2007, ApJ, 666, 955)

4. Discussion

- Influence of dust on the elemental composition of the second-generation stars
- Extinction curve in the early universe

1. Introduction

1-1. Cosmic dust

○ **ダスト** : 宇宙空間中に存在する固体微粒子

銀河系のダスト: **graphite**と**silicate grains**

$$n(a) = f(a)da = a^{-3.5} da \quad (0.001 \sim 1 \mu\text{m})$$

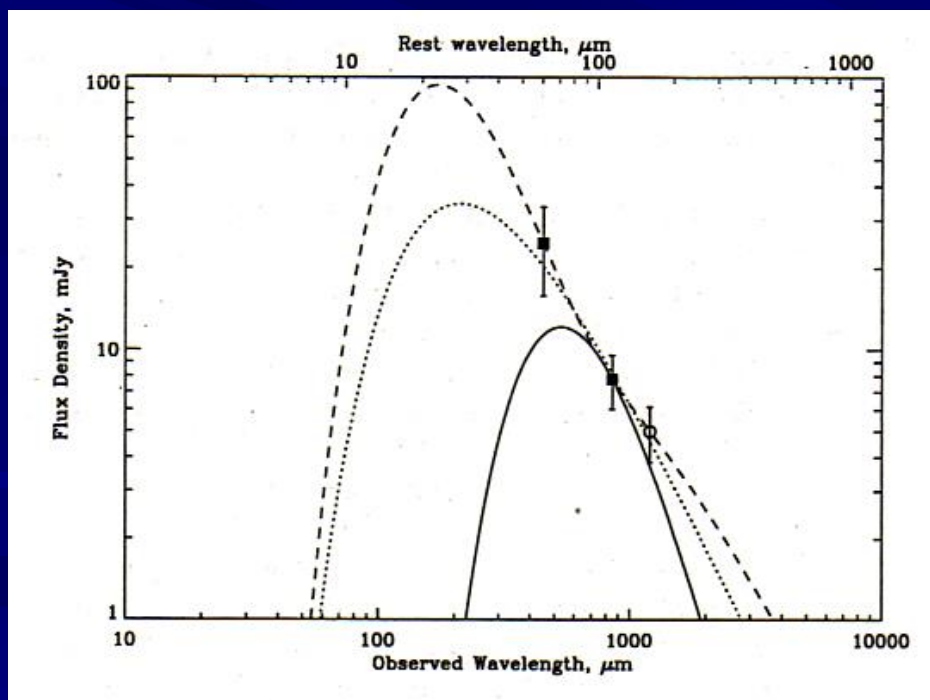
$$M_{\text{dust}} / M_{\text{gas}} \sim 1 / 140$$

- 星からの光(紫外・可視光)を吸収し、得たエネルギーを熱放射として(赤外線で)放出する
- **ダストの形成場所**
 - 豊富な重元素、低温 ($T < \sim 2000 \text{ K}$)、高密度 ($n > 10^8 \text{ cm}^{-3}$)
 - AGB星のmass-loss wind中
 - 重力崩壊型超新星爆発時に放出されるガス中
 - 新星、赤色巨星、原始太陽系星雲、分子雲 ...

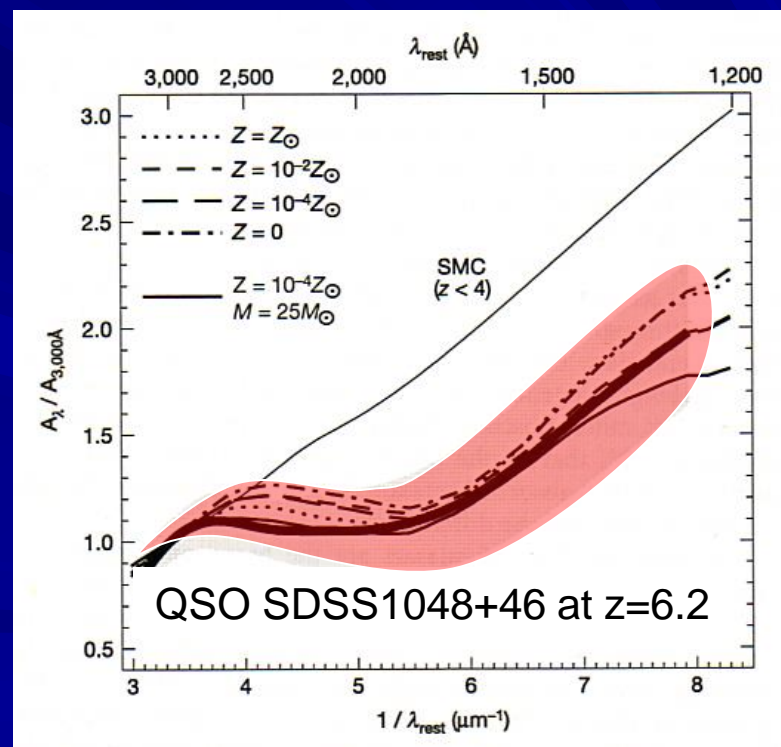
1-2. Dust in the early universe

○ 高赤方偏移のダストの観測

- $z > 6$ (< 1 Gyr) の宇宙初期にも大量 ($> 10^8 M_{\odot}$) のダストを確認
(Bertoldi et al. 2003; Robson et al. 2004; Beelen et al. 2006)
- 宇宙初期のダストの性質は、銀河系やその近傍のものとは異なっている？



QSO SDSS J1148+52 at $z=6.4$
(Robson et al. 2004)



(Maiolino et al. 2004)

1-3. Role of dust in the early universe

○ 宇宙初期のダストの役割

- ・ 観測からSFRやIMFを推定する際に大きな影響を及ぼす
- ・ 星や銀河の形成・進化史に重要な役割を果たす
 - － 星間空間中のエネルギーバランスを制御
 - － ダストの表面上での(水素)分子の形成
 - － metal-poorな環境で低質量星の形成を促進

Population III stars : $> 100 M_{\odot}$

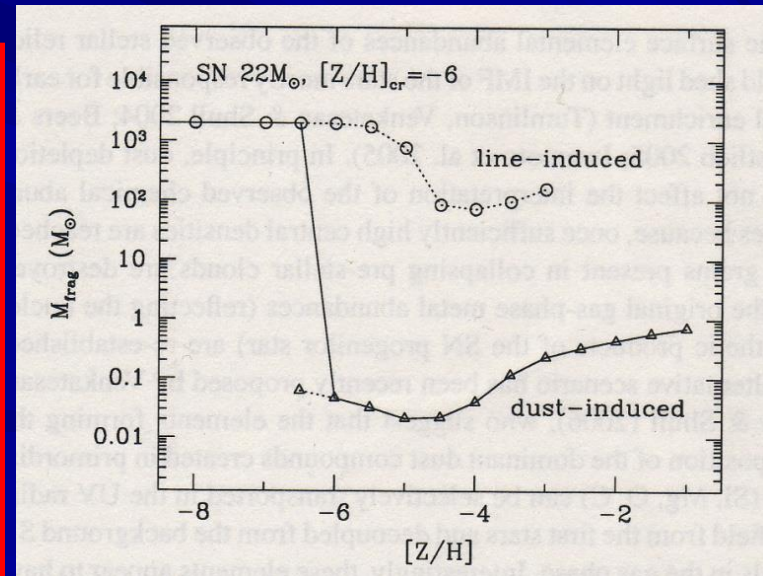
Population II stars : $\sim 1 M_{\odot}$

critical metallicity Z_{crit}

$$Z_{\text{crit}} = 10^{-4} - 10^{-3} Z_{\odot} \text{ for } f_{\text{dep}} = 0$$

$$Z_{\text{crit}} = 10^{-6} - 10^{-4} Z_{\odot} \text{ for } f_{\text{dep}} = 0.2$$

($f_{\text{dep}} = M_{\text{dust}} / M_{\text{metal}}$; depletion factor)



(Schneider et al. 2006)

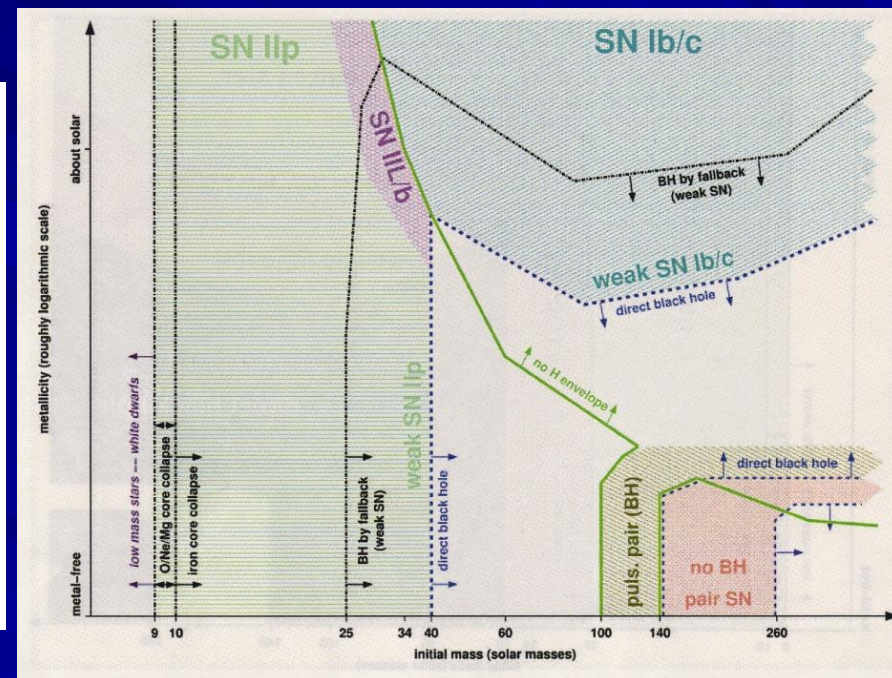
1-4. Motivation

ダストによる光の吸収・熱放射の効率は、星間空間中に存在するダストの種類やサイズ、存在量に大きく依存する

宇宙初期における星や銀河の進化を考察するには、宇宙初期のダストの性質を明らかにすることが必要不可欠！

○ 宇宙初期のダストの供給源

- Type II SNe (SNe II)
; $M_{pr}=8-40 M_{\odot}$
- pair-instability SNe (PISNe)
; $M_{pr}=140-260 M_{\odot}$



(Heger et al. 2003)

1-5. Aim of our study

- 宇宙初期のダストの主要な形成場所は、大質量星の進化の結果として起こる超新星爆発時に放出されるejecta中
- 超新星爆発時に形成されたダストは、星間空間中に放出される際、ejecta中を伝搬するreverse shockにより破壊される

ダストの破壊効率は大質量星の種類やサイズに依存する



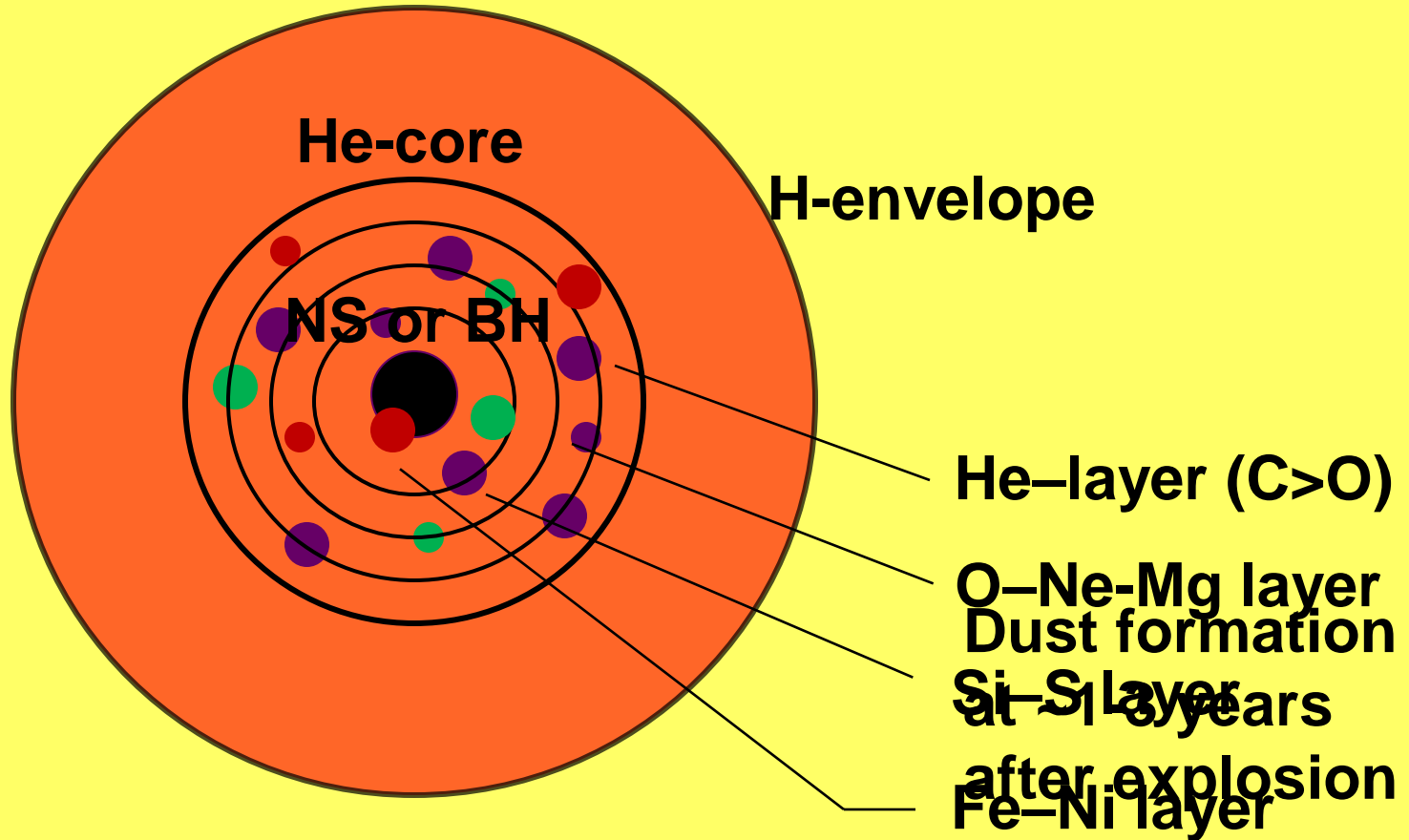
ダストの形成と破壊の素過程を統合的に取り扱い、宇宙初期の超新星爆発時に星間空間中に供給されるダストの種類やサイズ、量を明らかにする

本計算は超新星残骸(SNR)の観測の比較から超新星爆発時でのダストの形成とSNR中のダストの物理進化過程を明らかにする上でも重要

2. Dust formation in the ejecta of Population III supernovae

2-1. Dust formation in the ejecta of SNe

at ~1 days



2-2-1. Calculations of dust formation

○ ダスト形成理論 (Kozasa & Hasegawa 1987)

凝縮時の化学反応を考慮した、核形成・成長理論

・ key species

反応する原子(分子)のうち
最も衝突頻度がちいさいもの

ガスの元素組成
ガスの温度・密度の時間進化



形成するダストのサイズや量を決定

Table 2. Grain species considered in the calculations

Dust species	Chemical reactions
Fe _(s)	Fe _(g) → Fe _(s)
FeS _(s)	Fe _(g) + S _(g) → FeS _(s)
Si _(s)	Si _(g) → Si _(s)
Ti _(s)	Ti _(g) → Ti _(s)
V _(s)	V _(g) → V _(s)
Cr _(s)	Cr _(g) → Cr _(s)
Co _(s)	Co _(g) → Co _(s)
Ni _(s)	Ni _(g) → Ni _(s)
Cu _(s)	Cu _(g) → Cu _(s)
C _(s)	C _(g) → C _(s)
SiC _(s)	Si _(g) + C _(g) → SiC _(s)
TiC _(s)	Ti _(g) + C _(g) → TiC _(s)
Al ₂ O _{3(s)}	2Al _(g) + 3O _(g) → Al ₂ O _{3(s)}
MgSiO _{3(s)}	Mg _(g) + SiO _(g) + 2O _(g) → MgSiO _{3(s)}
Mg ₂ SiO _{4(s)}	2Mg _(g) + SiO _(g) + 3O _(g) → Mg ₂ SiO _{4(s)}
SiO _{2(s)}	SiO _(g) + O _(g) → SiO _{2(s)}
MgO _(s)	Mg _(g) + O _(g) → MgO _(s)
Fe ₃ O _{4(s)}	3Fe _(g) + 4O _(g) → Fe ₃ O _{4(s)}
FeO _(s)	Fe _(g) + O _(g) → FeO _(s)

2-2-2. Calculations of dust formation

Steady-state nucleation rate

$$J_j^s(t) = \alpha_{sj} \Omega_j \left(\frac{2\sigma_j}{\pi m_{1j}} \right)^{1/2} \left(\frac{T}{T_d} \right)^{1/2} \Pi_j c_{1j}^2 \exp \left[-\frac{4}{27} \frac{\mu_j^3}{(\ln S_j)^2} \right],$$

Supersaturation ratio

$$\ln S_j = -\frac{\Delta G_j^0}{kT} + \sum_i \nu_{ij} \ln P_{ij},$$

α_s : sticking probability of key species ($\alpha_s = 1$, in the calculations)

Ω : volume of the condensate per key species

σ : surface energy of the condensate

m_1 : mass of key species

c_1 : number density of key species

μ : $\mu \equiv 4\pi a_0^2 \sigma / kT$; energy barrier for nucleation

2-2-3. Calculations of dust formation

Equation of conservation for key species

$$1 - \frac{c_{1j}(t)}{\tilde{c}_{1j}(t)} = 1 - Y_{1j} = \int_{t_e}^t \frac{J_j(t')}{\tilde{c}_{1j}(t')} \frac{4\pi}{3\Omega_j} r_j^3(t, t') dt',$$

Equation of grain growth

$$\frac{dr_j}{dt} = \alpha_{sj} \Omega_j \left(\frac{kT}{2\pi m_{1j}} \right)^{1/2} c_{1j}(t) = \frac{1}{3} a_{0j} \tau_{\text{coll},j}^{-1}(t) r_j^3.$$



- the number density of dust grains, n_{gr}

$$\frac{n_{\text{gr}}}{\tilde{c}_1(t)} = \int_{t_0}^t \frac{J(t')}{\tilde{c}_1(t')} dt'$$

- the radius of dust grain nucleated at t_0 and measured at t

$$r(t, t_0) = a_0 + \int_{t_0}^t \frac{1}{3} a_0 \tau_{\text{coll}}^{-1}(t') dt'$$

2-2-4. Calculations of dust formation

○ Pop III SNe のモデル (Umeda & Nomoto 2002)

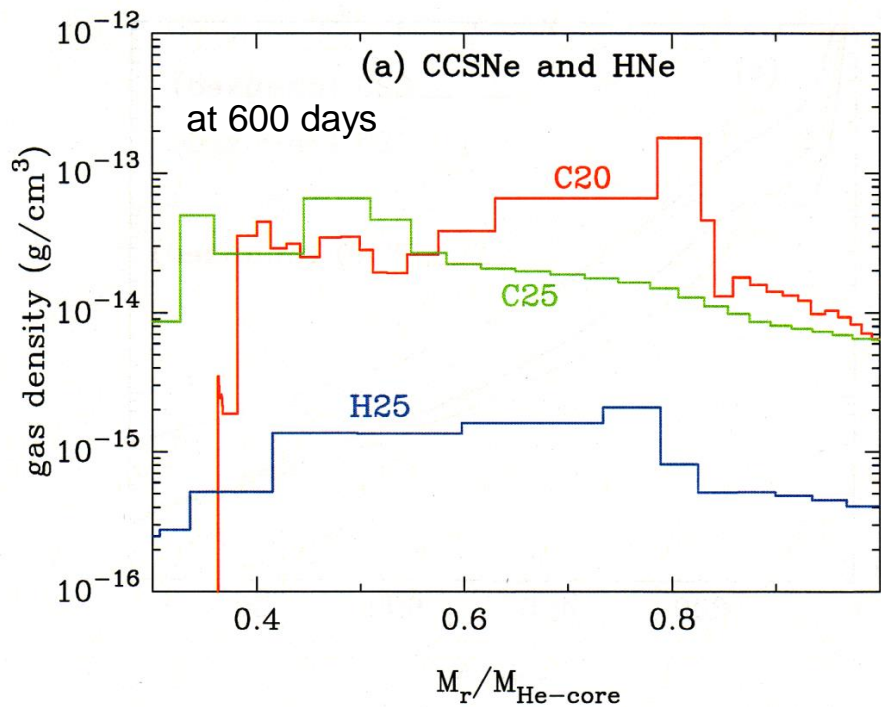
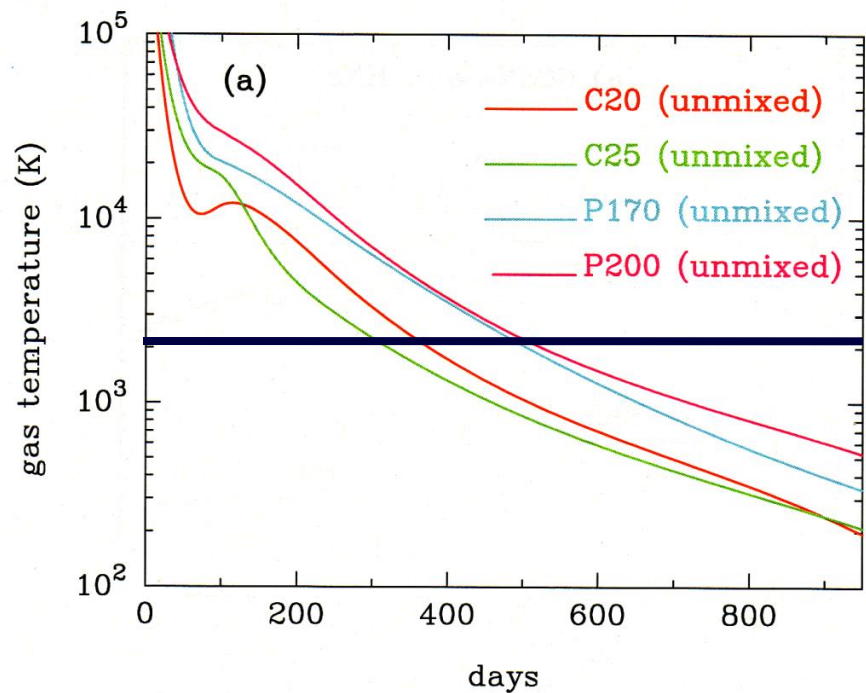
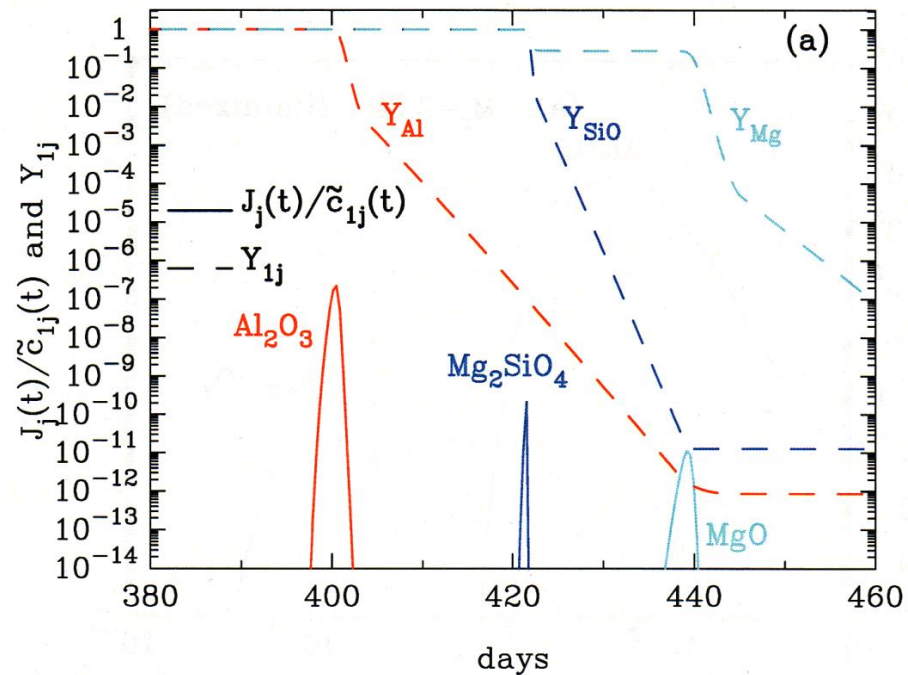
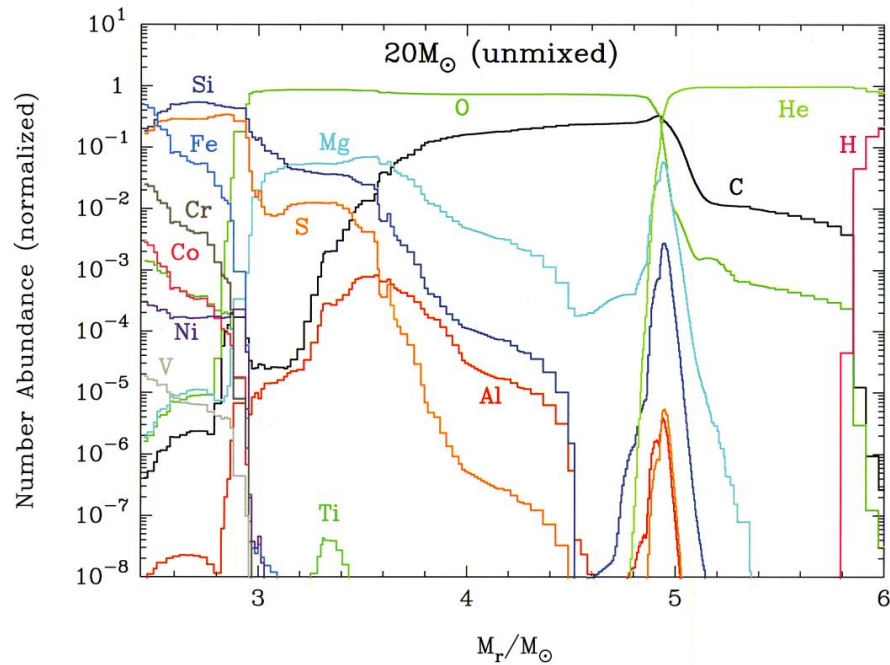
- SNe II : $M_{\text{pr}} = 13, 20, 25, 30 M_{\odot}$
- PISNe : $M_{\text{pr}} = 150, 170, 200 M_{\odot}$

○ He-core中の元素組成

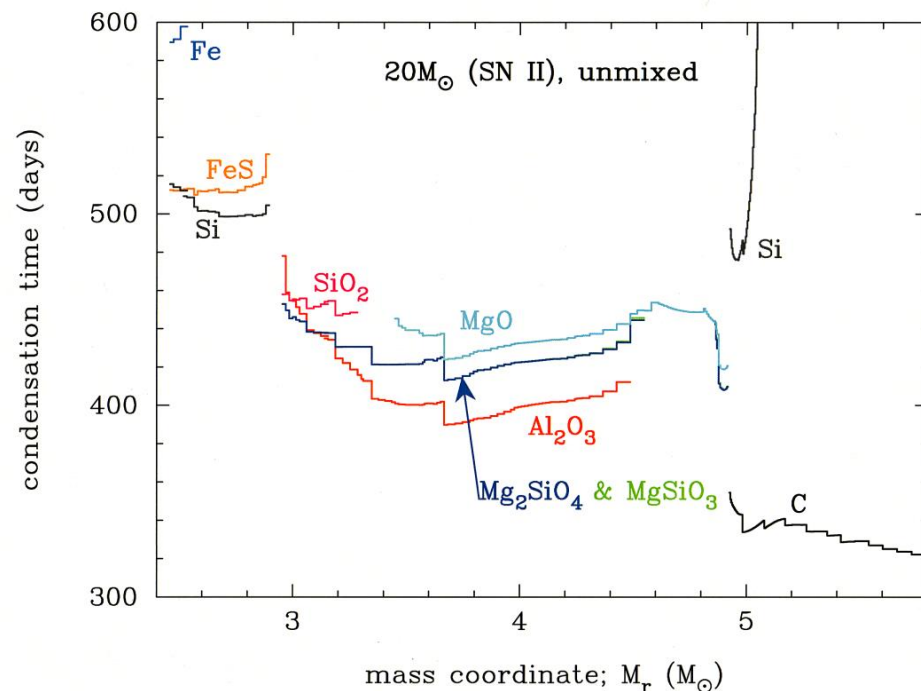
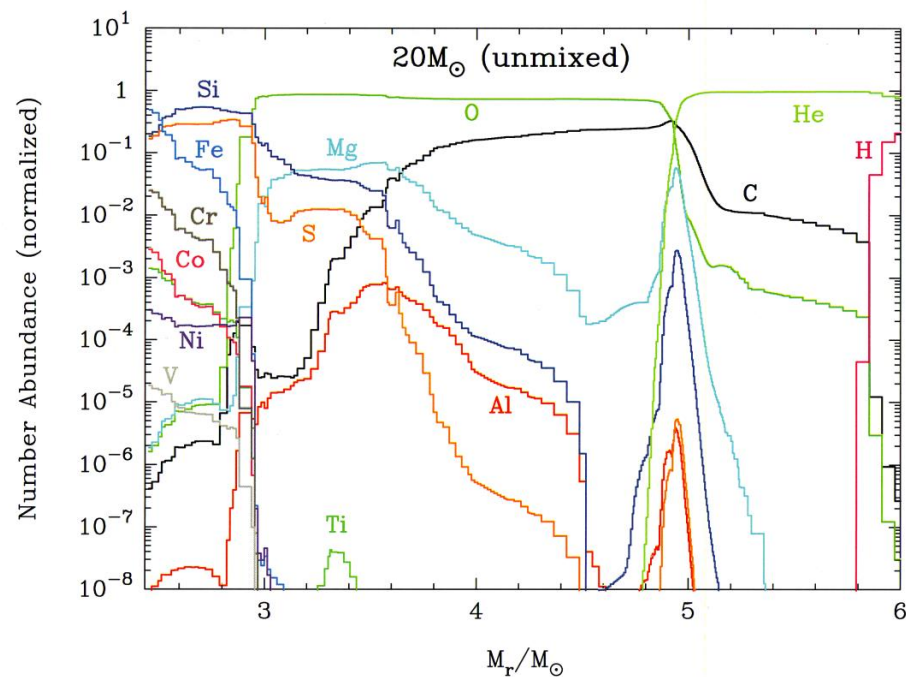
- 元素の混合が起こっていない場合 (unmixed case)
- He-core中で均一に混合させた場合 (mixed case)

○ CO, SiO分子の形成

- $C/O < 1 \rightarrow$ すべてのCがCOに
- $C/O > 1 \rightarrow$ すべてのOがCOに
- $Si/O < 1 \rightarrow$ すべてのSiがSiOに

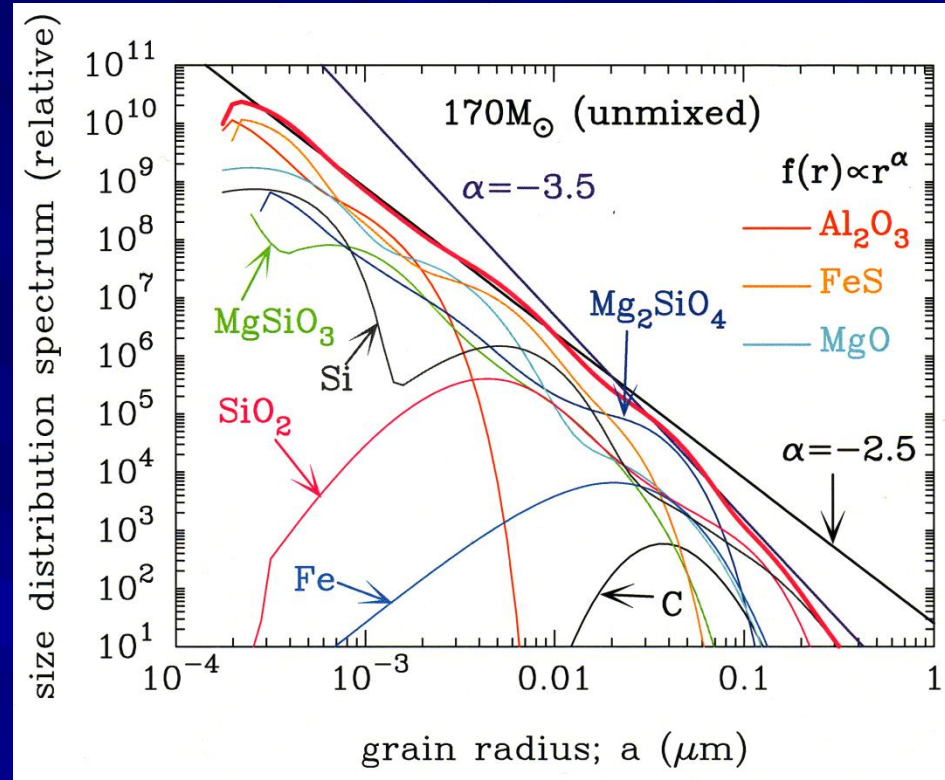
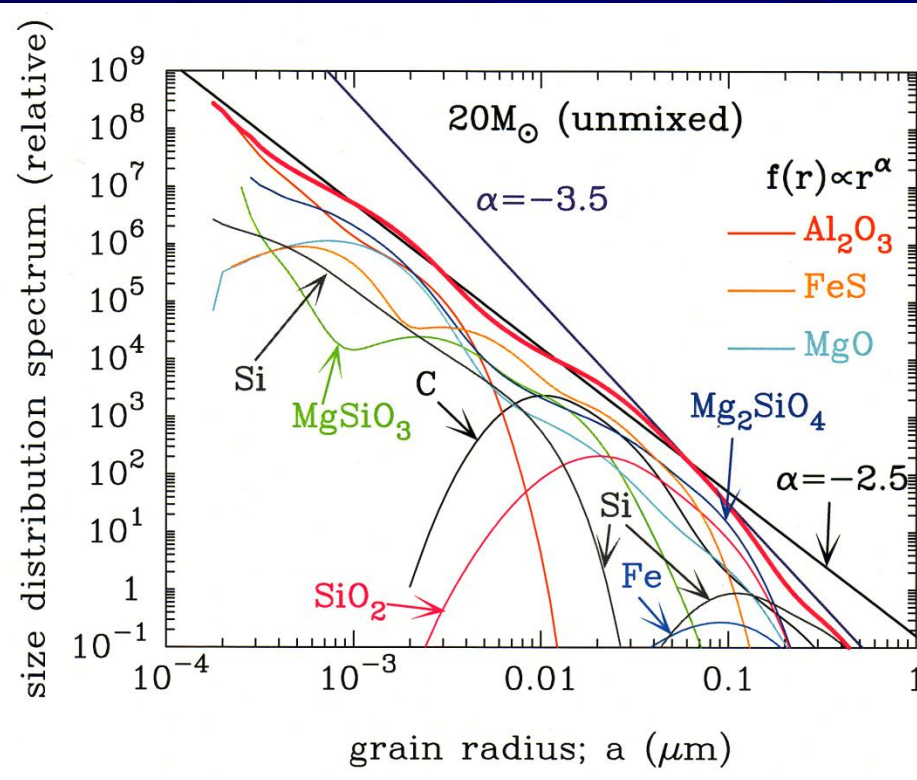


2-3. Dust formation in the unmixed ejecta



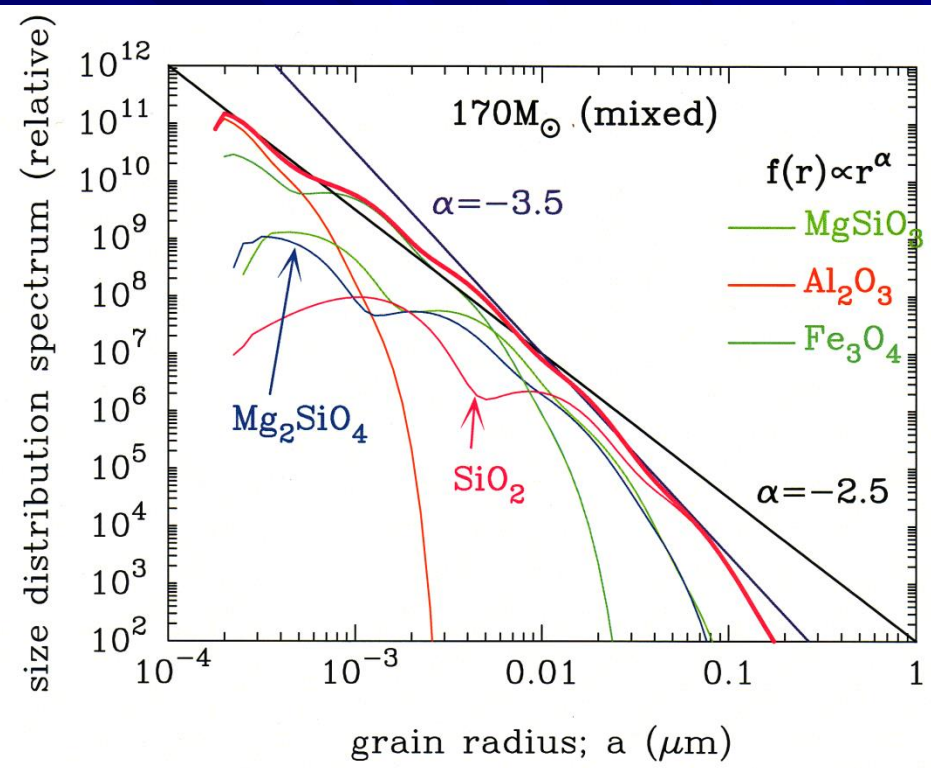
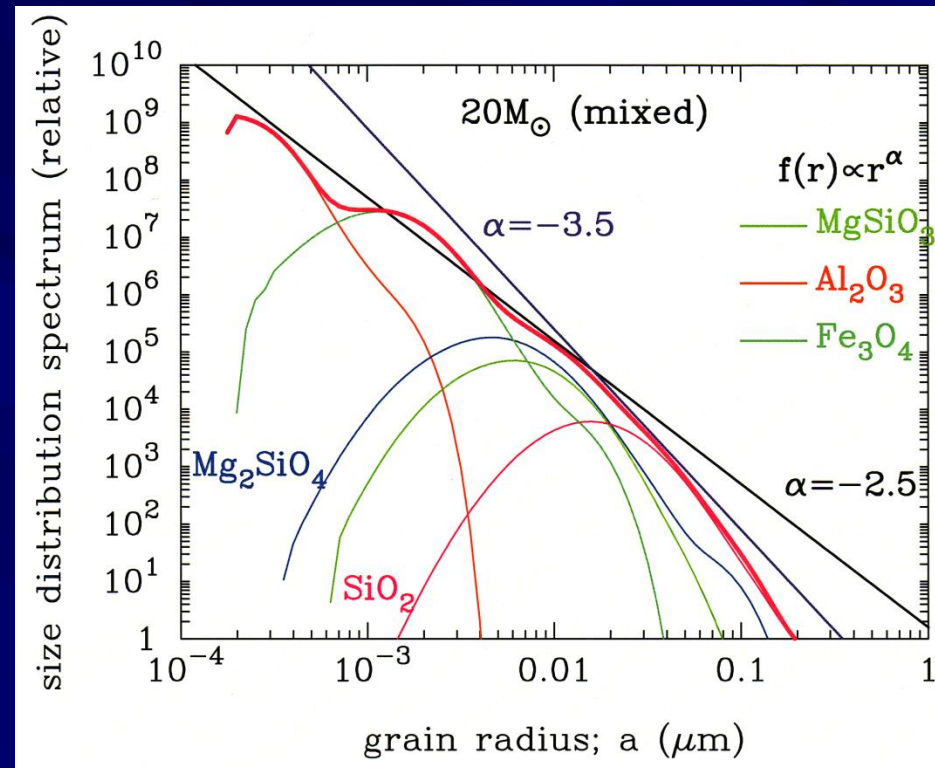
- He-core中の元素組成の違いに応じて、さまざまな種類 (Fe, Si, FeS, SiO₂, Al₂O₃, MgSiO₃, Mg₂SiO₄, MgO, C) のダストが形成
- ダストは爆発後300-600日で形成される

2-4. Dust formed in the unmixed ejecta



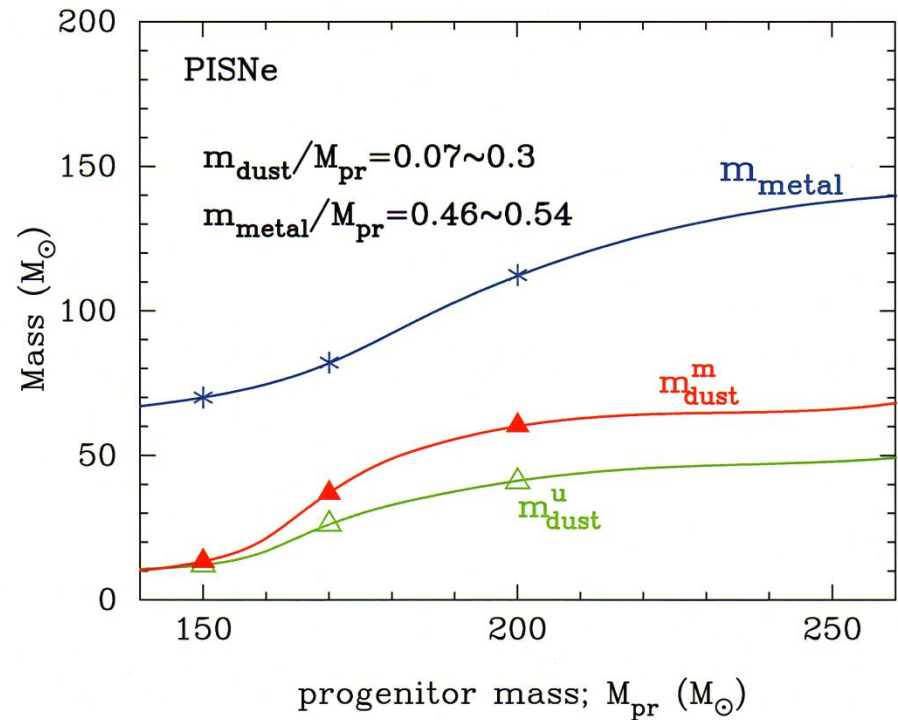
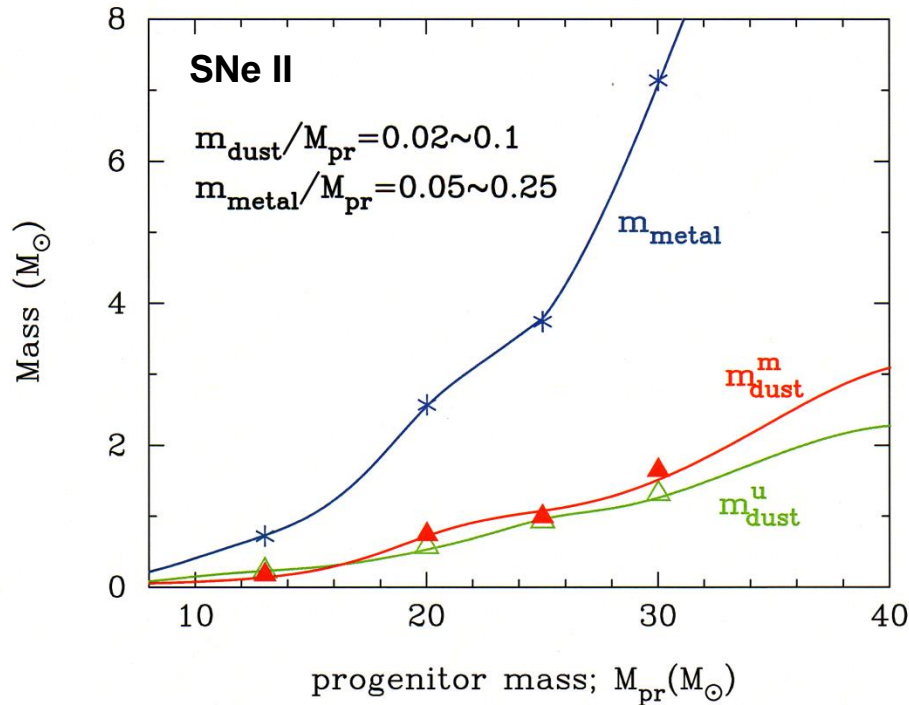
- ・ 各ダスト種のサイズ分布は、近似的にlognormalかpower-law
- ・ 形成されるダストの種類やすべてのダスト種にわたって足し合わせたサイズ分布は、前駆星の質量に依存しない

2-5. Dust formed in the mixed ejecta



- He-core全体がO-richとなり、silicate (MgSiO₃, Mg₂SiO₄, SiO₂)と酸化物 (Fe₃O₄, Al₂O₃)が形成される
- 各ダスト種のサイズ分布は、Al₂O₃を除いてlognormal-like

2-6. Total mass of dust formed



- ・ダストの全質量は、前駆星の質量が増加するほど増加する
SNe II : $M_{\text{dust}} = 0.1-2 M_{\odot}$ PISNe : $M_{\text{dust}} = 10-60 M_{\odot}$
- ・元素の混合を均一にさせた場合の方が、元素の混合がない場合よりもダスト量は多い

2-7. Summary of dust formation

○ 形成されるダストの種類

- unmixed case

C, Si, Fe, FeS, Al_2O_3 , MgSiO_3 , Mg_2SiO_4 , SiO_2 , MgO

- mixed case

MgSiO_3 , Mg_2SiO_4 , SiO_2 , Fe_3O_4 , Al_2O_3

○ 形成されるダストのサイズ

- 各ダスト種のサイズ分布は, lognormalかpower-law分布
- 全ダストを足し合わせたサイズ分布は, broken power-law

○ 形成されるダストの量

- 前駆星の質量が増加するほど全ダスト量は増加する

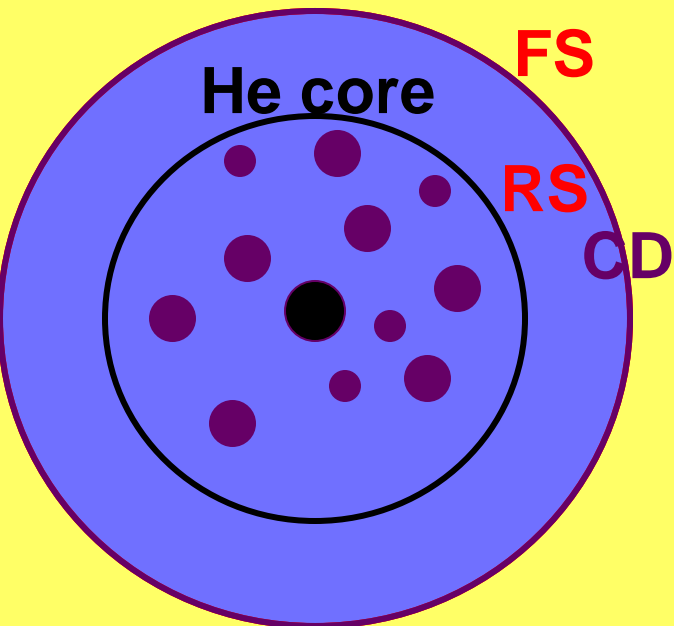
SNe II : $M_{\text{dust}} = 0.1-2 M_{\odot}$

PISNe : $M_{\text{dust}} = 10-60 M_{\odot}$

3. Dust evolution in Population III supernova remnants

3-1. Dust evolution in a SN remnant

$$T = (1-2) \times 10^4 \text{ K}$$
$$n_{\text{H}} = 0.1-1 \text{ cm}^{-3}$$



3-2-1. Time evolution of shock wave

- Basic equations (spherical symmetry)

$$\frac{\partial \rho}{\partial t} + \frac{1}{r^2} \frac{\partial}{\partial r} (r^2 \rho v) = 0$$

$$\frac{\partial}{\partial t} (\rho v) + \frac{1}{r^2} \frac{\partial}{\partial r} (r^2 \rho v^2) = -\frac{\partial P}{\partial r}$$

$$\begin{aligned} \frac{\partial}{\partial t} \left(\frac{\rho v^2}{2} + \frac{P}{\gamma - 1} \right) + \frac{1}{r^2} \frac{\partial}{\partial r} \left(r^2 \left[\frac{\rho v^2}{2} + \frac{\gamma P}{\gamma - 1} \right] v \right) \\ = - (n_e n_H \Lambda_{\text{gas}}(T) + \Lambda_{\text{ic}}(T) + \Lambda_{\text{d}}(n_H, T)) \end{aligned}$$

$\Lambda_{\text{gas}}(T)$: cooling function of gas by the atomic process

(Sutherland & Dopita 1993; Smith et al. 2001)

$\Lambda_{\text{ic}}(T)$: inverse Compton cooling (Ikeuchi & Ostriker 1986)

$$\Lambda_{\text{ic}}(T) = 5.41 \times 10^{-32} (1+z)^4 n_e (T/10^4 \text{ K}) \quad (\text{we adopt } z = 20)$$

$\Lambda_{\text{d}}(n_H, T)$: cooling of gas through thermal emission of dust

- numerical code : flux splitting method (van Albada et al. 1982)

3-2-2. Initial condition for shock wave

○ SN ejecta model (Umeda & Nomoto 2002)

- SNe II : $M_{\text{pr}}=13, 20, 25, 30 M_{\odot}$ ($E_{51}=1$)
- PISNe : $M_{\text{pr}}=170$ ($E_{51}=20$), $200 M_{\odot}$ ($E_{51}=28$)
 - He-core中のガスは、Oのみからなると仮定

○ The ambient medium

- primordial composition (uniform)
- gas temperature ; $T = 10^4$ K
- gas density ; $n_{\text{H},0} = 0.1, 1, \text{ and } 10 \text{ cm}^{-3}$
(e.g., Kitayama et al. 2004; Machida et al. 2005)

The calculation is performed from 10 yr up to $\sim 10^6$ yr

3-3. Dynamics of dust

- ・ダストは球形とし、test particleとして扱う
- ・磁場はないと仮定し、ダストの電荷の効果は無視する

- deceleration of dust due to drag force (Baines et al. 1965)

$$\frac{dw_d}{dt} = \frac{F_{\text{drag}}}{m_d} = -\frac{3n_H kT}{2a\rho_d} \sum_i A_i G_i(s_i) \quad (w_d : \text{relative velocity})$$

ρ_d ; bulk density of a grain

A_i ; the number abundance of gas species i normalized by n_H

$$G_i(s_i) \approx \frac{8s_i}{3\sqrt{\pi}} \left(1 + \frac{9\pi}{64}s_i^2 \right)^{\frac{1}{2}} \quad (\text{Draine \& Salpeter 1979})$$

where $s_i^2 = m_i w_d^2 / 2kT$

3-4-1. Erosion rate of dust by sputtering

- dust destruction by sputtering (e.g., Dwek, Foster & Vancura 1996)

$$\frac{da}{dt} = -\frac{m_{\text{sp}}}{4\pi a^2 \rho_d} \sum_i \mathcal{R}(Y_i(E))$$

$Y_i(E) = 2Y_i^0(E)$; the angle-averaged sputtering yield

m_{sp} ; average mass of the sputtered atoms

- rate equation over a modified Maxwellian distribution of gas taken account of relative velocity of dust to gas (e.g., Shull 1978)

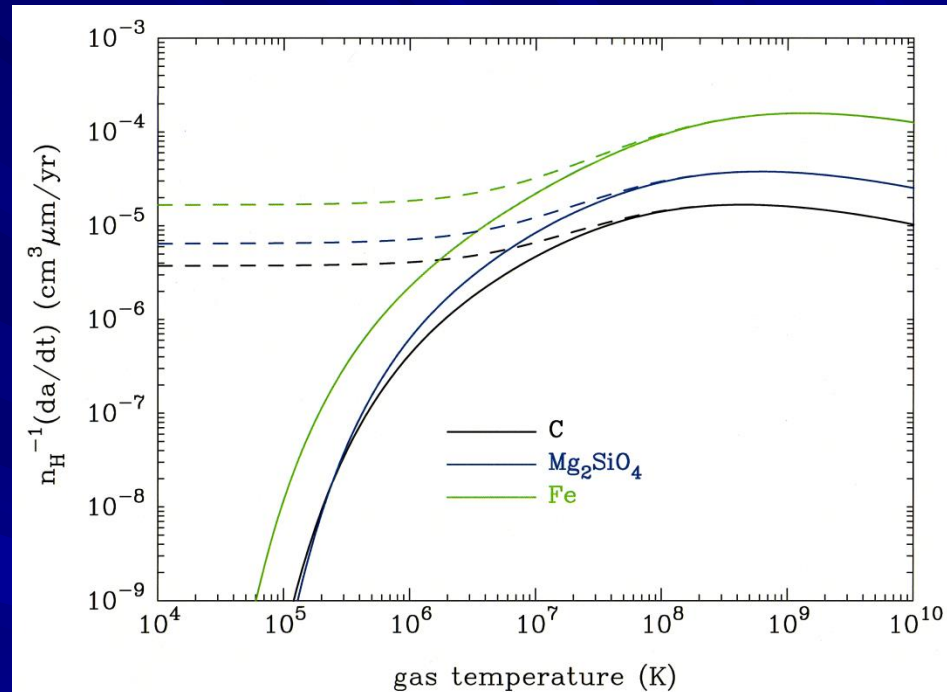
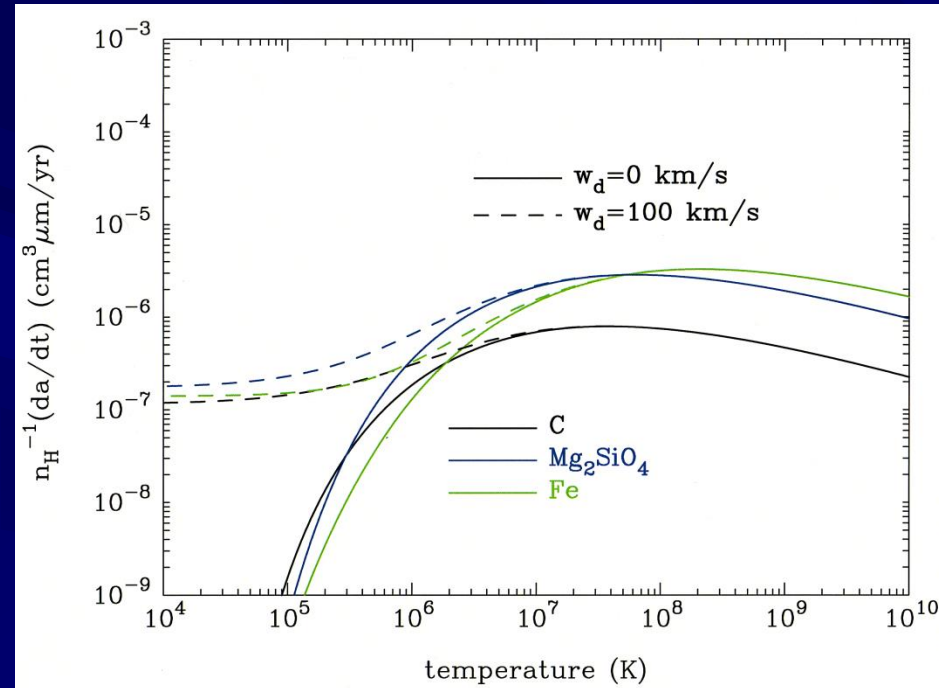
$$\mathcal{R}(X_i(\epsilon)) = n_{\text{H}} A_i \pi a^2 \left(\frac{8kT}{\pi m_i} \right)^{\frac{1}{2}} \frac{e^{-s_i^2}}{2s_i} \int \sqrt{\epsilon} e^{-\epsilon} \sinh(2s_i \sqrt{\epsilon}) X_i(\epsilon) d\epsilon$$

where $\epsilon = E/kT$

3-4-2. Erosion rate of dust by sputtering

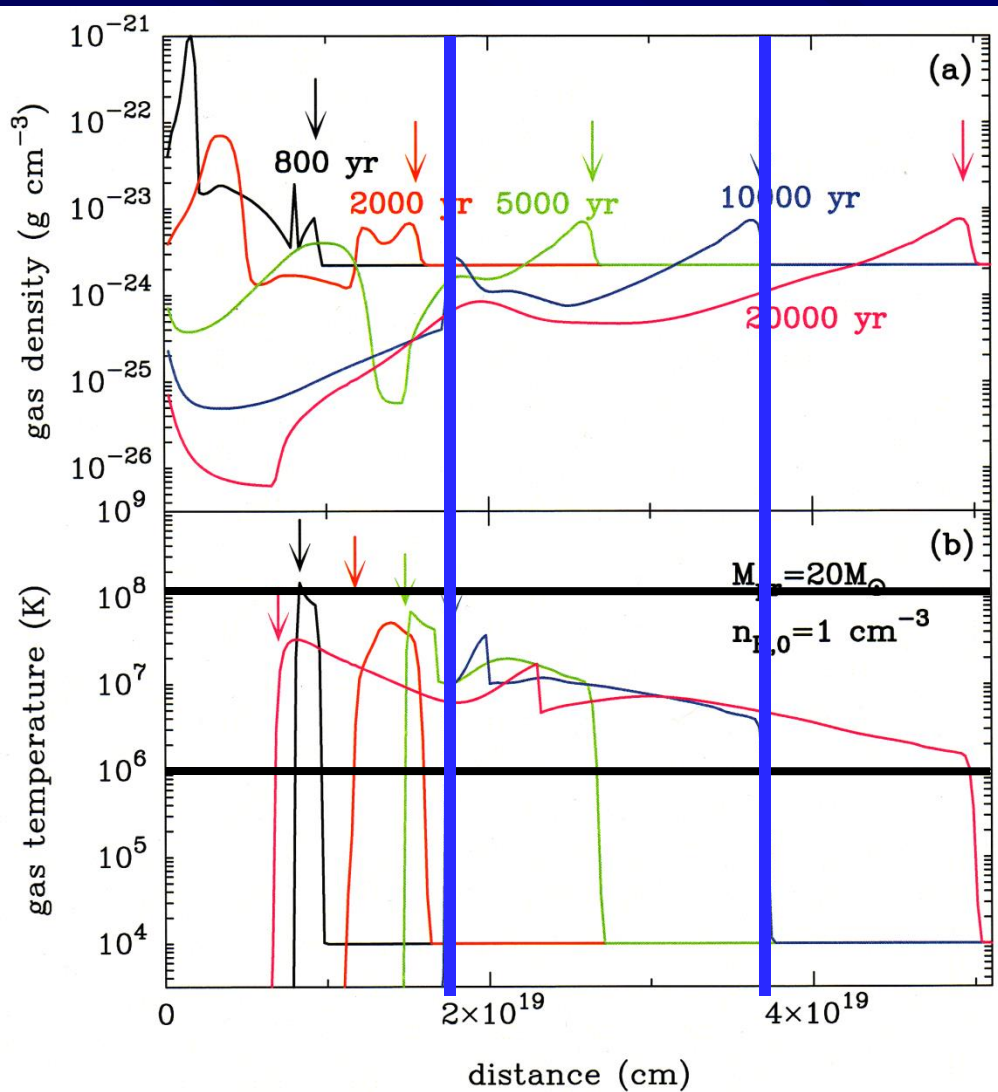
projectile ; primordial composition gas

projectile ; oxygen ions



- sputteringによるerosion rateは、 10^5 K から急激に増加し、 10^7 Kから 10^8 K でピークをもつ
- $da / dt \sim 10^{-6} n_H \mu\text{m yr}^{-1}$ for $T > 10^6$ K

3-5. Temperature and density of gas



Model : $M_{\text{pr}} = 20 M_{\odot}$ ($E_{51} = 1$)
 $n_{\text{H},0} = 1 \text{ cm}^{-3}$

Downward-pointing arrows:
forward shock in upper panel
reverse shock in lower panel

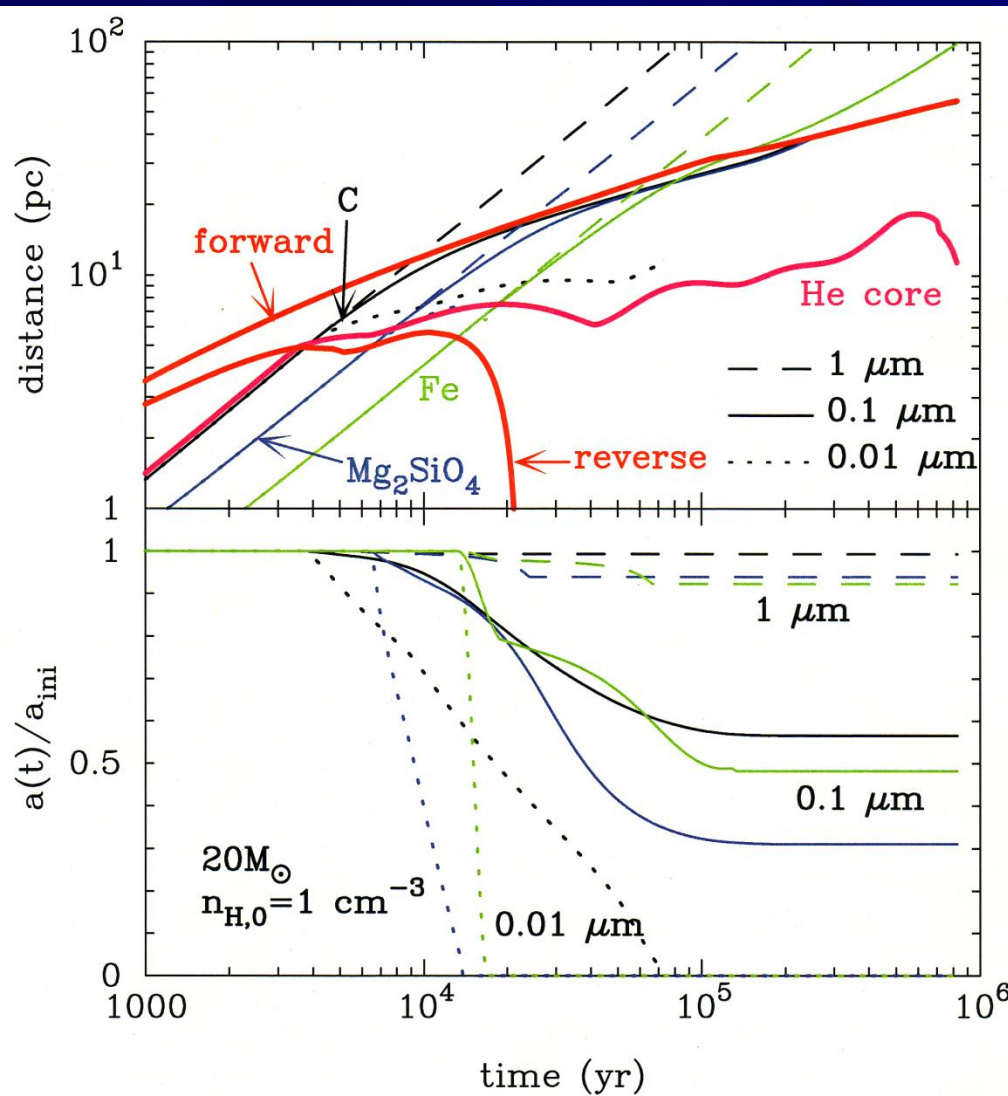
The temperature of the gas
swept up by the shocks

→ $10^6 - 10^8 \text{ K}$



Dust grains residing in this hot
gas are eroded by sputtering

3-6. Evolution of dust in SNRs



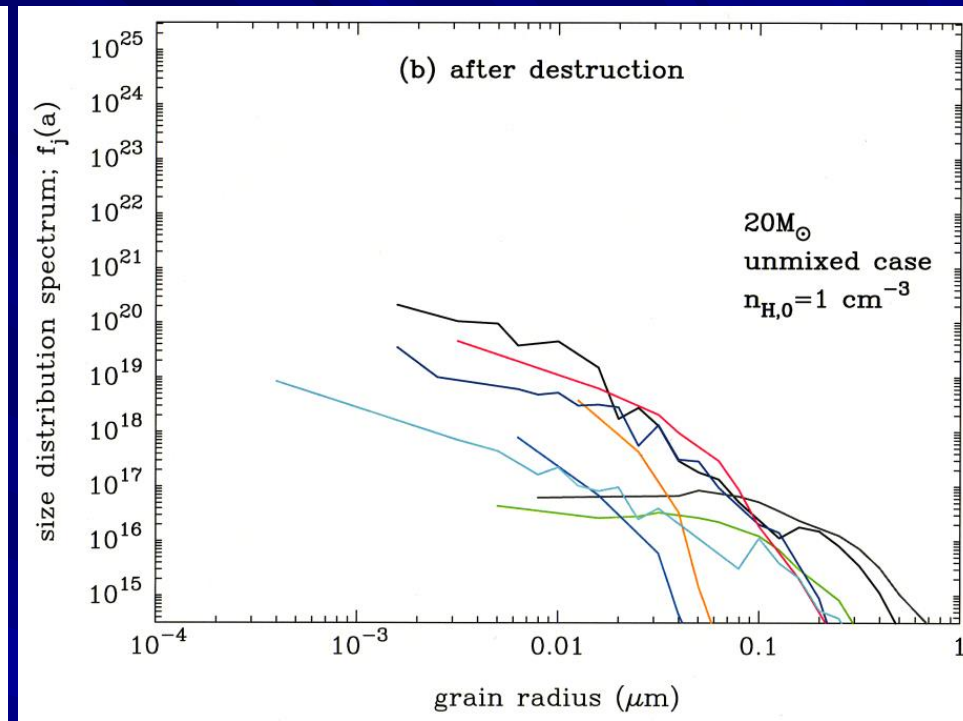
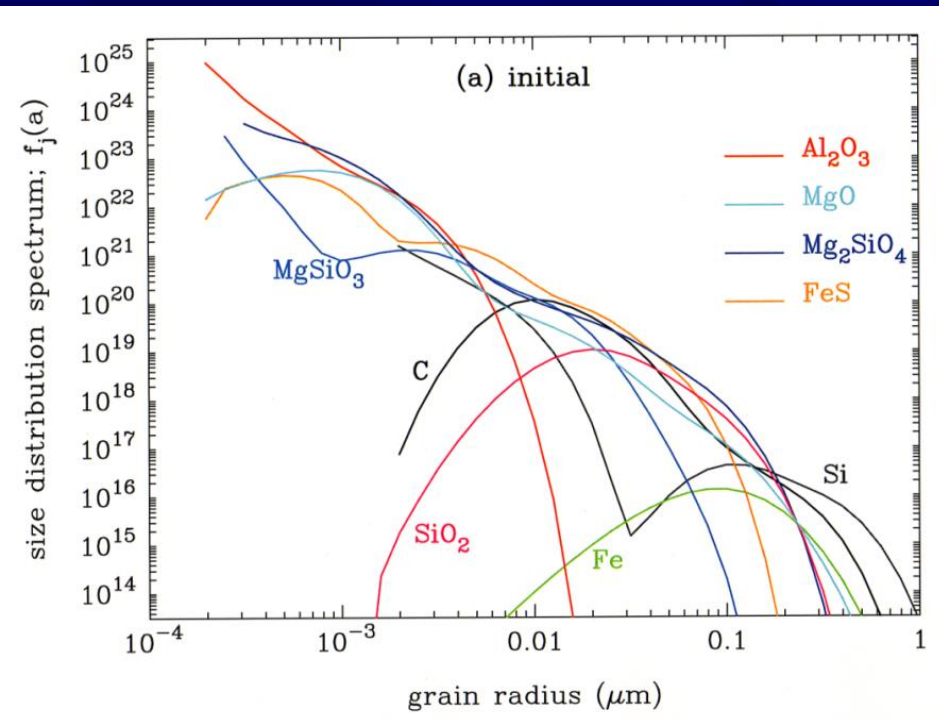
Model : $M_{pr} = 20 M_{\odot}$ ($E_{51} = 1$)
 $n_{H,0} = 1 \text{ cm}^{-3}$

Dust grains in the He core collide with reverse shock at $(3-13) \times 10^3 \text{ yr}$

The evolution of dust heavily depends on the initial radius and composition

- $a_{ini} = 0.01 \mu m$ (dotted lines)
→ completely destroyed
- $a_{ini} = 0.1 \mu m$ (solid lines)
→ trapped in the shell
- $a_{ini} = 1 \mu m$ (dashed lines)
→ injected into the ISM

3-7. Size distribution of surviving dust

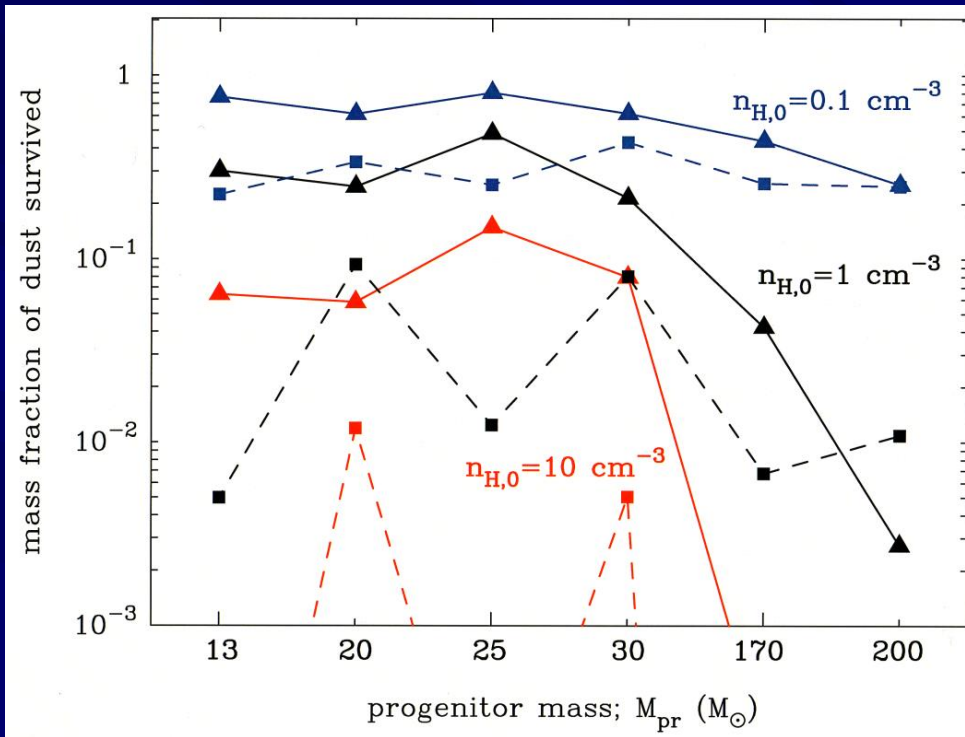


The size distribution of surviving dust is greatly deficient in small-sized grains, compared with that at its formation

→ Dust in the early universe is dominated by large-sized grains

The evolution of dust within SNRs is almost independent on the progenitor mass as long as explosion energy is the same.

3-8. Total mass fraction of surviving dust



星間空間中の密度が大きいほど、
生き残るダストの質量は小さい

完全に破壊されるダストの初期サイズ

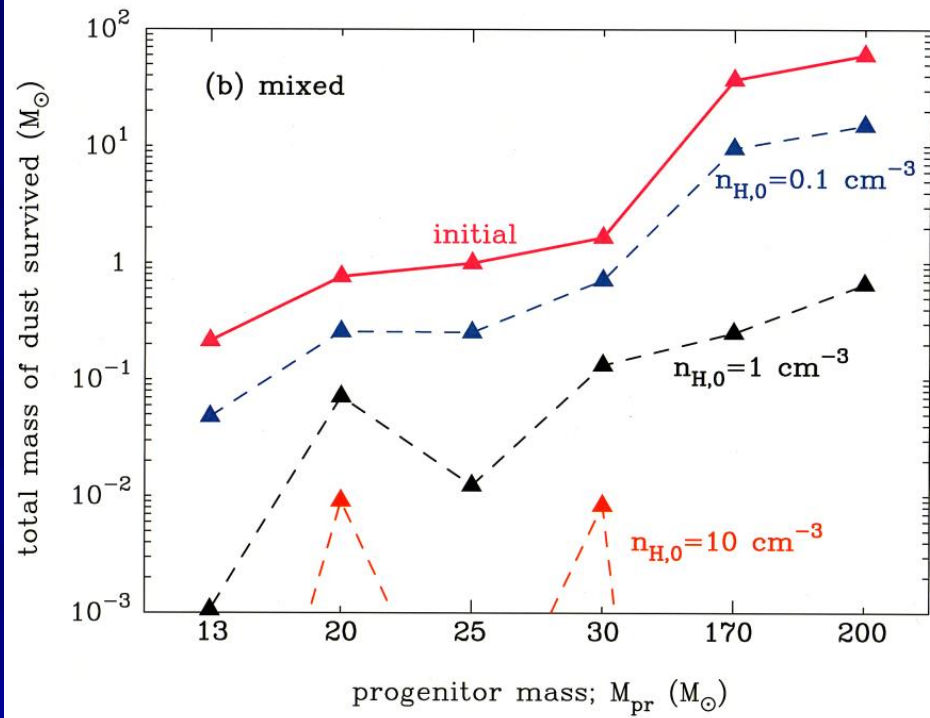
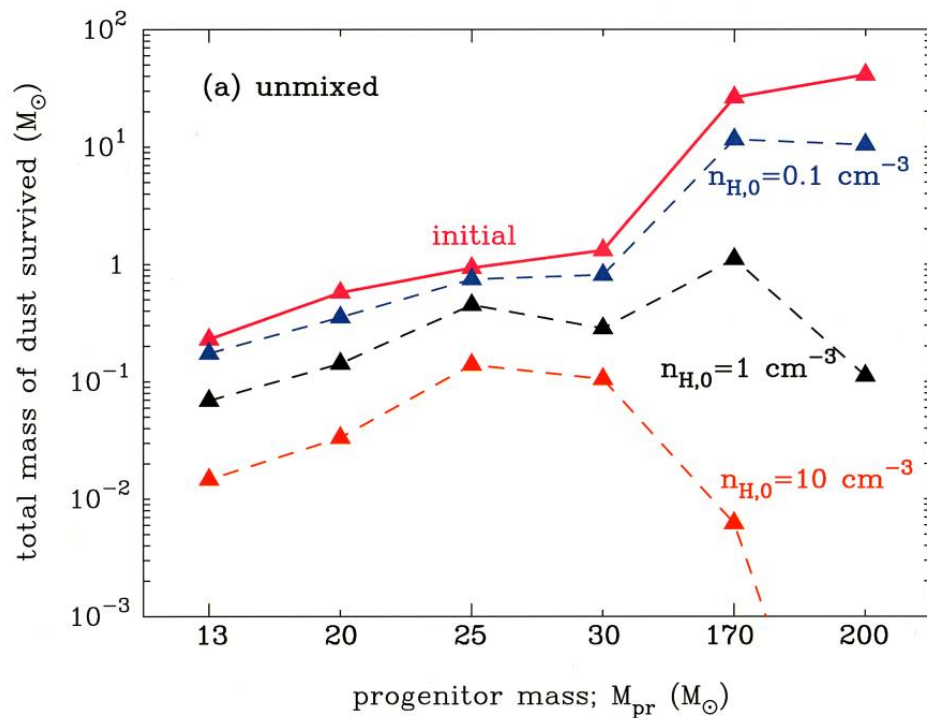
$a_{\text{ini}} < \sim 0.01 \mu\text{m}$ for $n_{\text{H},0} = 0.1 \text{ cm}^{-3}$

$a_{\text{ini}} < \sim 0.05 \mu\text{m}$ for $n_{\text{H},0} = 1 \text{ cm}^{-3}$

$a_{\text{ini}} < \sim 0.2 \mu\text{m}$ for $n_{\text{H},0} = 10 \text{ cm}^{-3}$

- mixed caseで形成されたダストはunmixed caseで形成されたダストよりも破壊されやすい
- PISNeで形成されたダストはSNe IIよりも破壊されやすい

3-9. Total mass of surviving dust



Total mass of dust surviving the destruction for Type II SNRs;
0.01-0.8 M_{\odot} for the unmixed grain model ($n_{\text{H},0} = 0.1-10 \text{ cm}^{-3}$)
0.001-0.7 M_{\odot} for the mixed grain model ($n_{\text{H},0} = 0.1-1 \text{ cm}^{-3}$)

0.1-1 M_{\odot} for SNe II and $n_{\text{H},0} = 0.1 \text{ cm}^{-3}$

→ high enough to explain the content of dust at high-z galaxies
(Morgan & Edmunds 2003, Maiolino et al. 2004; Dwek et al. 2007)

3-10. Summary of dust evolution in SNRs

- 超新星残骸内のダストの進化は、ダストの組成や初期サイズに大きく依存する
- 周囲のガスの密度 ($n_{\text{H},0} = 0.1-10 \text{ cm}^{-3}$) に依存して、 $0.01-0.2 \mu\text{m}$ よりサイズの小さいダストはsputteringにより破壊され、**形成時のサイズの大きいダスト種が支配的に供給される**
- 破壊されるダストのmass fractionは、周囲のガスの密度が大きいほど、爆発のエネルギーが大きいほど大きくなる

– 超新星爆発時に供給されるダストの質量

for $n_{\text{H},0} = 1-0.1 \text{ cm}^{-3}$

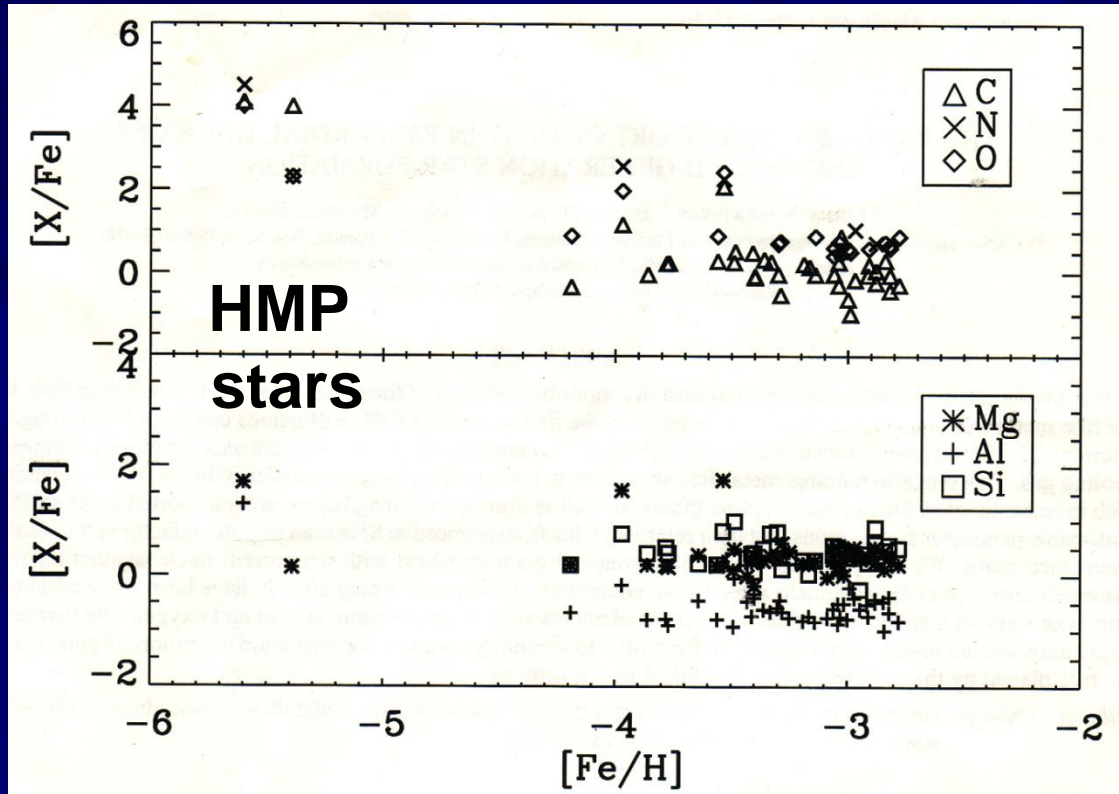
SNe II $\rightarrow M_{\text{dust}} = 0.01-0.8 M_{\odot}$ ($0.001-0.8 M_{\odot}$)

PISNe $\rightarrow M_{\text{dust}} = 0.1-15 M_{\odot}$

for $n_{\text{H},0} = 10 \text{ cm}^{-3}$, $M_{\text{dust}} < 0.1 M_{\odot}$ ($<0.01 M_{\odot}$)

4. Influence of dust on the elemental composition of the 2nd-generation stars

4-1. Abundance patterns of EMP stars



Venkatesan et al. (2006)

EMP stars ; $[Fe/H] < -3$
(extremely metal-poor stars)

UMP stars ; $[Fe/H] < -4$
(ultra metal-poor stars)

HMP stars ; $[Fe/H] < -5$
(hyper metal-poor stars)

$$[A/B] = \log_{10}(N_A/N_B) - \log_{10}(N_A/N_B)_{\odot}$$

- large overabundance of C, N, and O in HMP stars
- modest enhancement of Mg and Si in HMP stars

4-2. Origin of HMP stars

- mixing fallback in a core-collapse SN
(Umeda & Nomoto 2005; Iwamoto et al. 2005, Tominaga et al. 2006)
- nucleosynthesis and mass transfer in a first generation binary star
(Suda et al. 2004, Komiya et al. 2006)
- external pollution of gas with heavy elements
(Shigeyama et al. 2003)
- **dust transport scenario** (Venkatesan et al. 2006)
 - HMP stars are the second-generation stars formed in the shell of Pop III SNRs
 - Their abundance patterns are determined by the transport of newly formed dust driven by the UV radiation field

4-3. Elemental abundance in the shell (1)

dust grains surviving the destruction but not injected into the ambient medium are piled up in the dense shell in 10^5 - 10^6 yr



- the elemental composition of these piled-up grains
→ the elemental abundance of Population II.5 stars
- dust in the shell may enable the formation of stars with solar mass scales through thermal emission if $-6 < \log(Z/Z_{\odot}) < -4$
(Omukai et al. 2005; Schneider et al. 2006; Tsuribe & Omukai 2006)



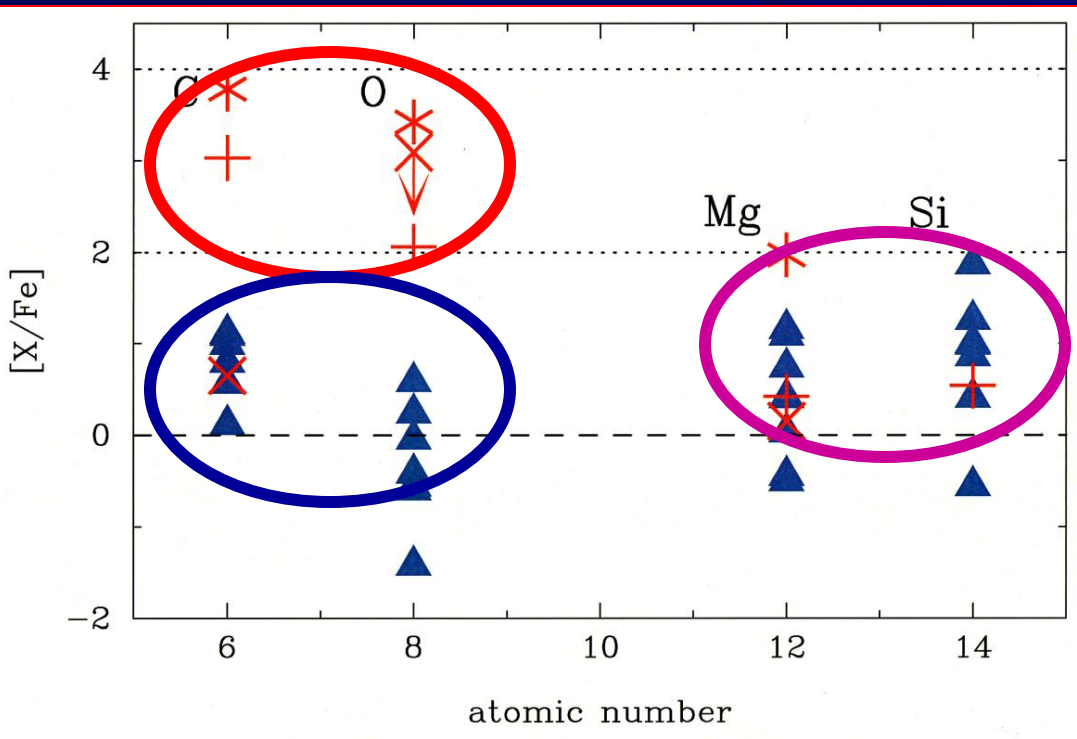
metallicity and metal abundance patterns in the shell
comparing with observations of HMP and UMP stars

4-4. Elemental abundance in the shell (1)

M_{pr} (M_{\odot})	[Fe/H]	[C/Fe]	[O/Fe]	[Mg/Fe]	[Si/Fe]	[Al/Fe]	[S/Fe]	$\log(Z/Z_{\odot})$
					$n_{\text{H},0} = 0.1 \text{ cm}^{-3}$			
13	-6.43	-0.274	-0.699	-0.230	1.52	2.00	0.255	-5.89
20	-5.20	0.117	-0.595	0.034	0.410	-1.97	0.242	-5.44
25	-5.90	1.11	-1.42	-0.500	-0.552	-0.563	0.242	-5.55
30	-5.56	0.566	-0.043	0.739	0.866	0.905	0.242	-5.33
					$n_{\text{H},0} = 1 \text{ cm}^{-3}$			
13	-5.15	1.11	-0.555	-0.459	1.01	-	-2.18	-4.72
20	-5.53	0.992	0.585	1.16	1.87	-	0.200	-4.68
25	-5.23	1.09	-0.412	0.407	0.989	-	0.241	-4.79
30	-5.11	0.797	0.242	1.09	1.26	-5.72	0.242	-4.60
					$n_{\text{H},0} = 10 \text{ cm}^{-3}$			
13	-4.13	[Fe/H] = -5.62 (HE0107-5240; Collet et al. 2006)						-4.40
20	-4.92	[Fe/H] = -5.96 (HE1327-2326; Frebel et al. 2008)						-4.09
25	-5.10	[Fe/H] = -4.75 (HE0557-4840; Noris et al. 2007)						-3.91
30	-5.11	3-D corrected						-3.84

critical metallicity
 $Z_{\text{cr}} = 10^{-6} - 10^{-4} Z_{\odot}$

4-5. Elemental abundance in the shell (3)



$$-6 < [Fe/H] < -5$$

$$0 < [Mg, Si/Fe] < 2$$

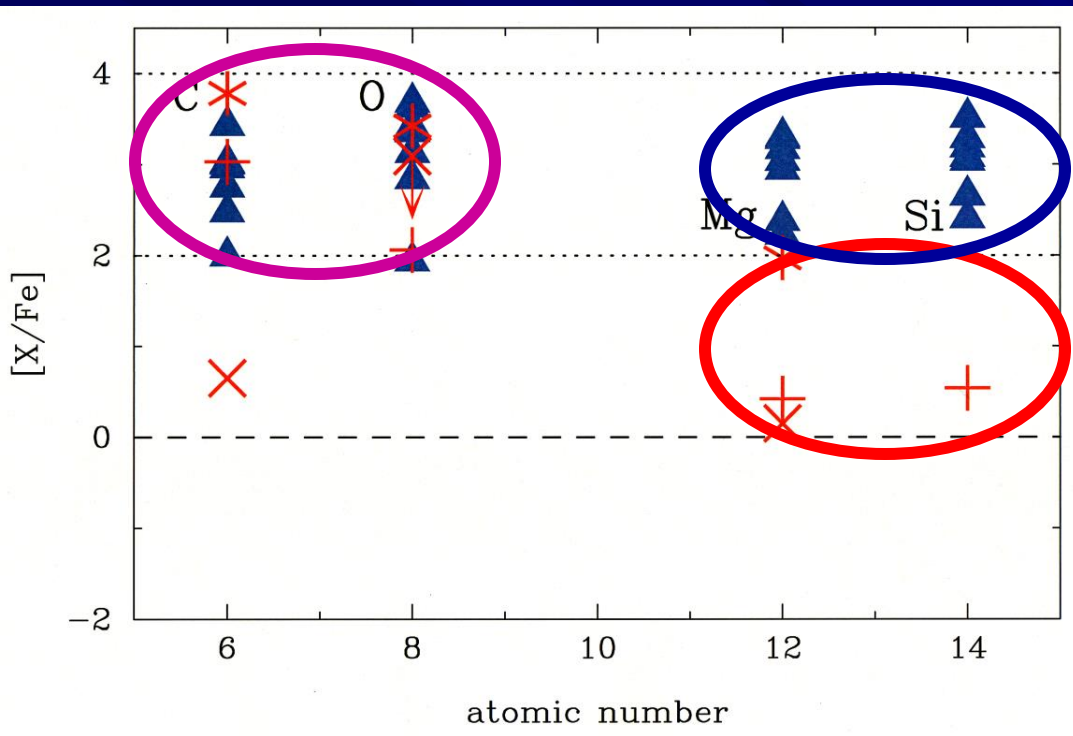


Elemental composition of dust piled up in the shell can reproduce abundance patterns in HMP stars

The transport of dust segregated from metal-rich gas can be responsible for the abundance patterns in HMP and UMP stars

more than 100 times excesses of C and O as observed in HMP and UMP stars cannot be reproduced

4-6. Elemental abundance in the shell (3)



We assume that the gas outside the innermost Fe layer in the ejecta is incorporated into the shell



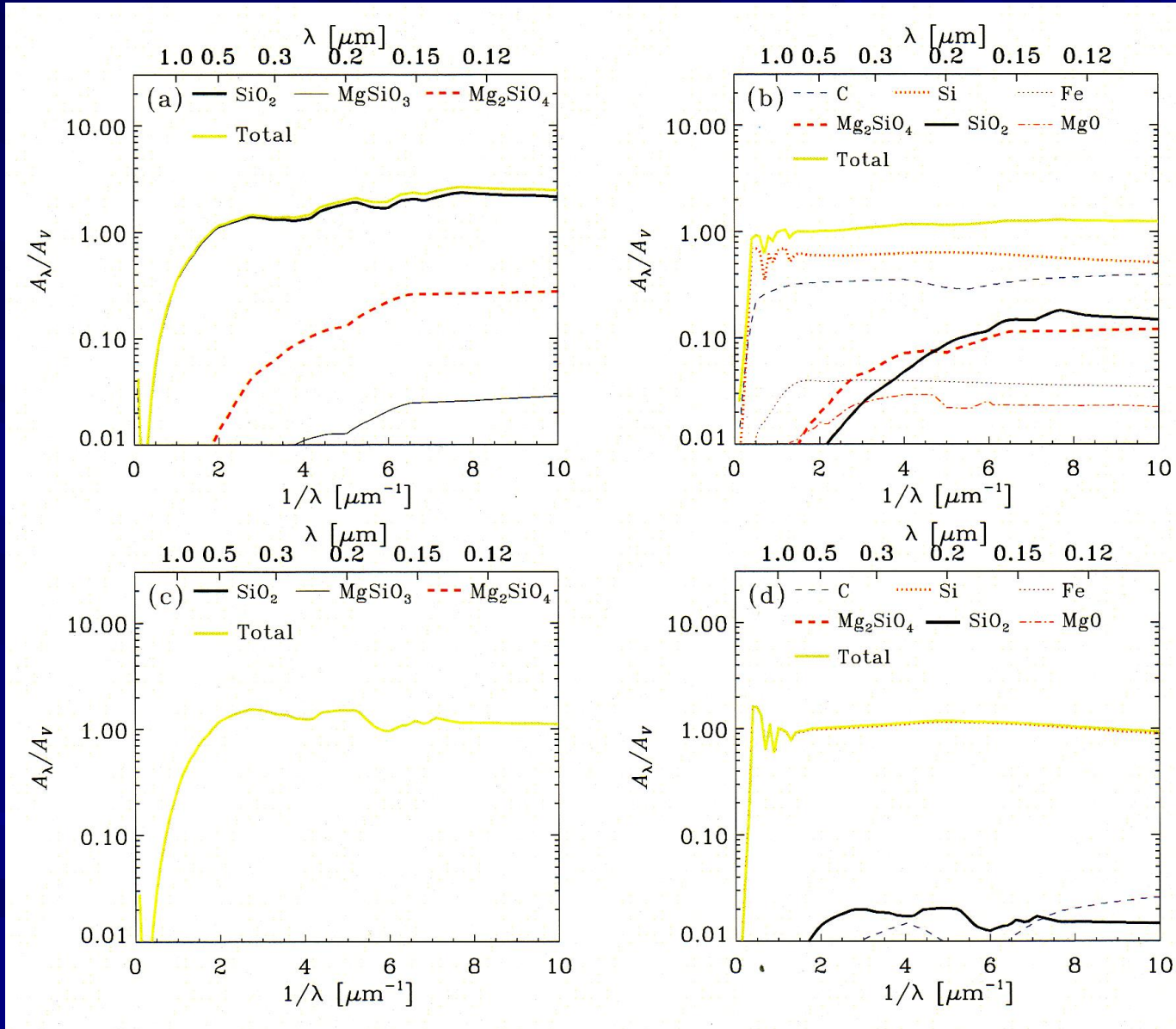
reproducing the extreme overabundance of C and O leading to more than 100 time excesses of Mg and Si

It might be possible to reproduce the elemental abundances of HMP stars if Si-Mg-rich layer is not mixed into the shell

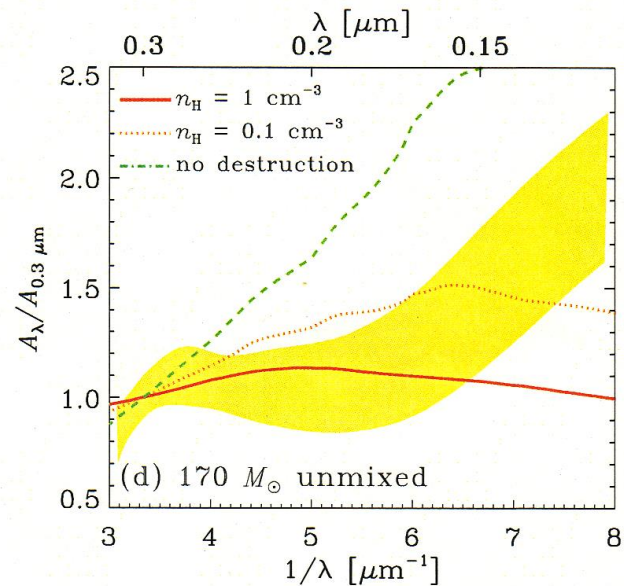
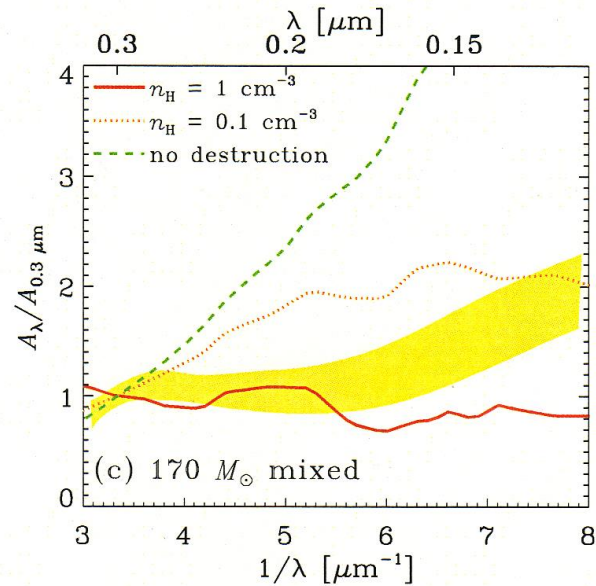
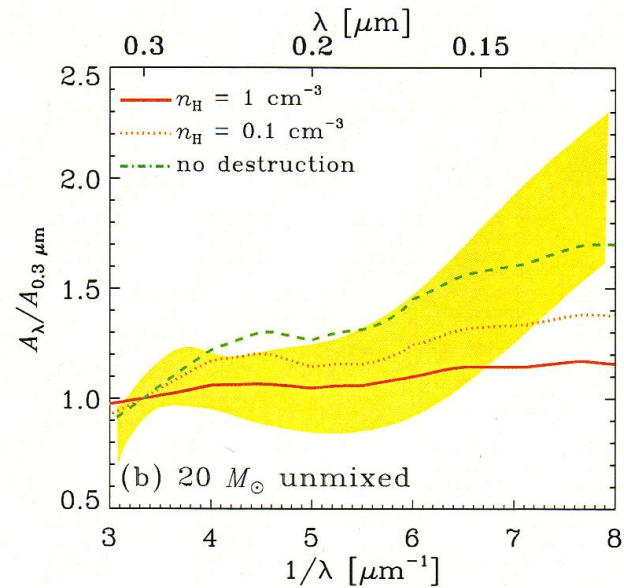
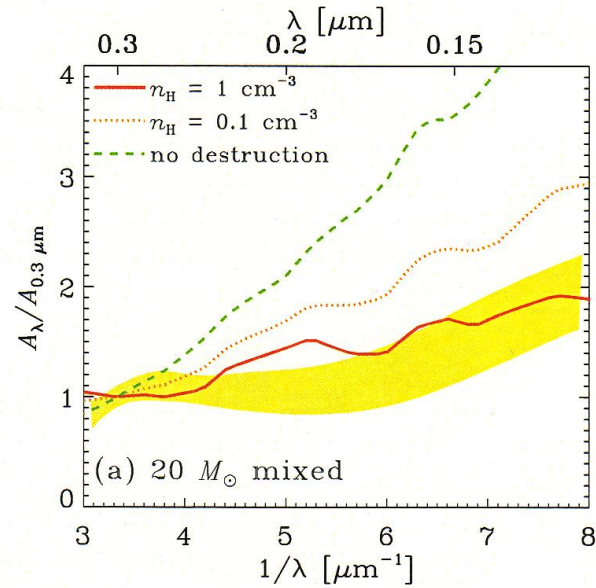
The transport of the newly formed dust within SNRs can be an important process to determine the metal abundance of the second generation stars formed in the Pop III SN shell

5. Extinction curves in the early universe

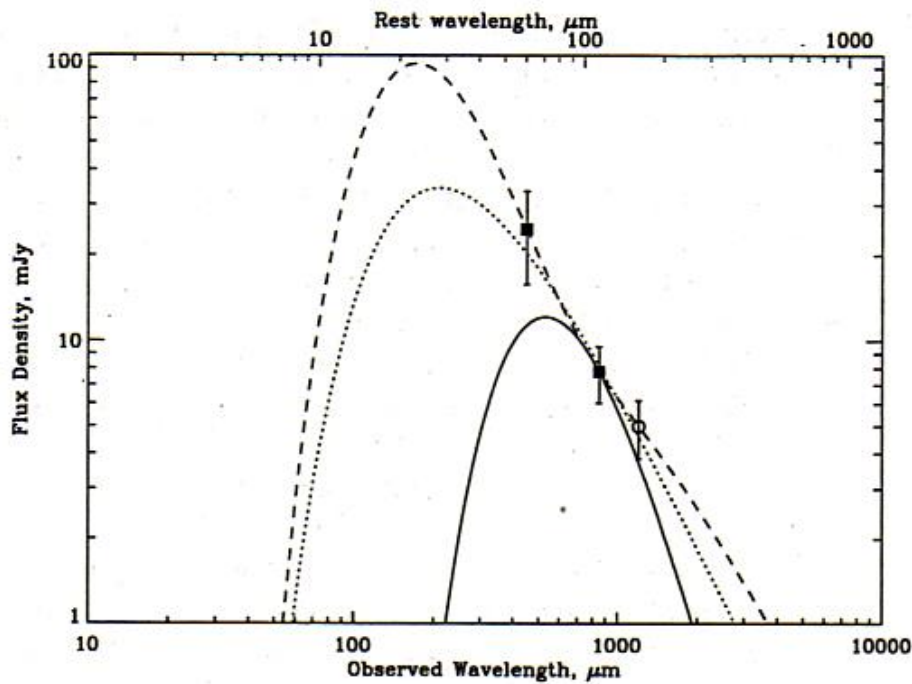
5-1. Flattened extinction curves (1)



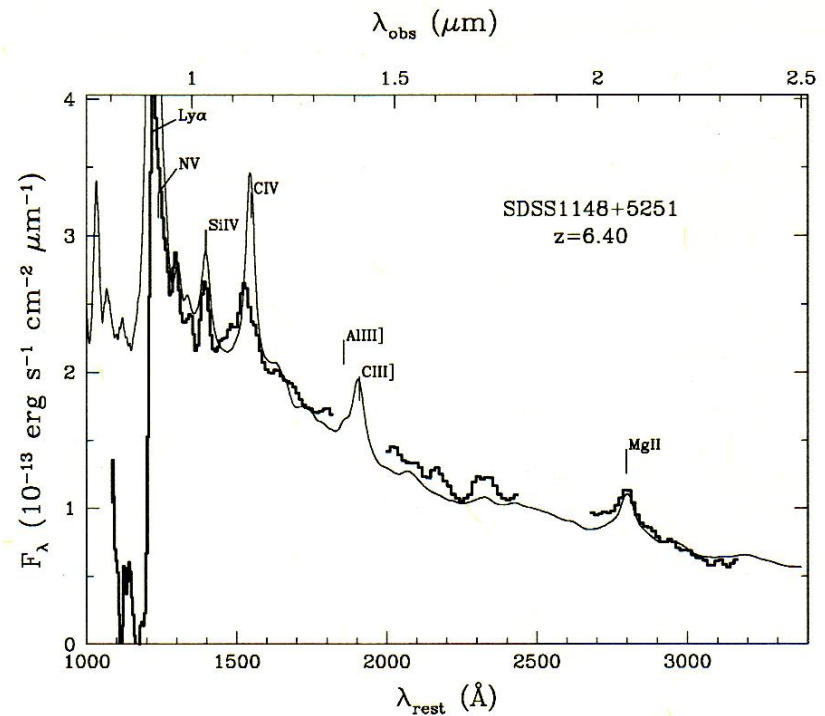
5-2. Flattened extinction curves (2)



5-3. Extinction in z=6.4 quasars



QSO SDSS J1148+52 at z=6.4
Robson et al.
(2004, MNRAS, 351, L29)



Maiolino et al.
(2004, A&A, 420, 889)

5-4. High-*z* quasars

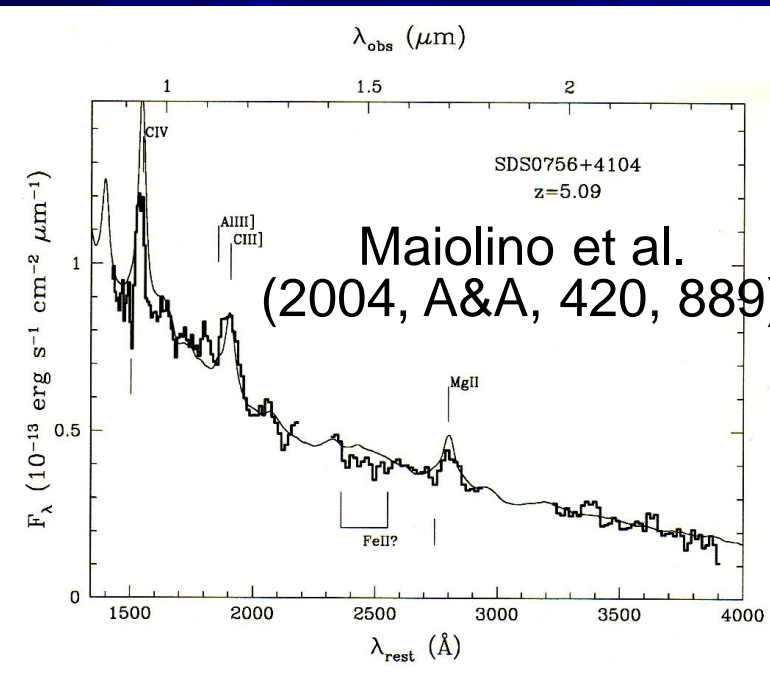
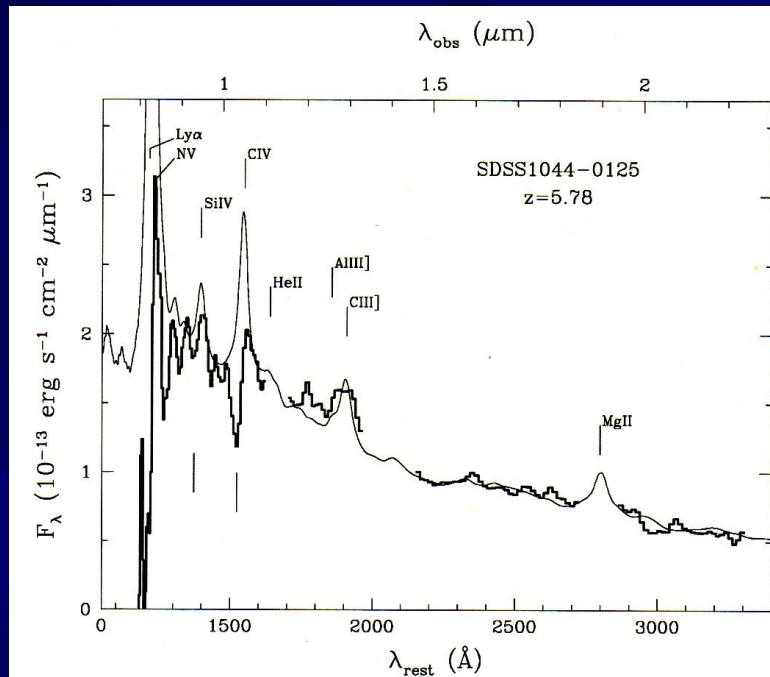
Name	<i>z</i>	Type	<i>BI</i> (CIV) ^a	α^b	<i>E</i> (<i>B</i> – <i>V</i>) ^c	<i>M</i> _{i*} ^d
SDSSJ075618.14+410408.6	5.08 ^e	BAL ^f	270 ± 60 ^g	–1.67	–	–26.6
SDSSJ103027.10+052455.0	6.28			–1.55	0.001	–28.1
SDSSJ104433.04-012502.2	5.78 ^h	HiBAL	1950 ± 250 ^g	–1.55	0.001	–28.4
SDSSJ104845.05+463718.3	6.22 ⁱ	LoBAL	6500 ± 1100 ^g	–2.10	– ^j	–27.4
SDSSJ114816.64+525150.3	6.40			–1.70	–	–28.5
SDSSJ130608.26+035626.3	5.99			–1.80	–	–27.8
SDSSJ160501.21-011220.6	4.92	LoBAL	9300 ± 2000 ^g	–1.35	0.03	–27.7
SDSSJ173744.88+582829.6	4.88 ^k			–2.10	–	–26.9

Maiolino et al. (2004, A&A, 420, 889)

Source	<i>z</i>	<i>M</i> _B	<i>S</i> _{850 μm} / <i>S</i> _{1.2 mm}	<i>S</i> _{450 μm} / <i>S</i> _{850 μm}	<i>t</i> (∞) – <i>t</i> (<i>z</i>) (Gyr)	<i>M</i> _d (10 ⁸ M _⊙)	<i>M</i> _* (min) (M _⊙ yr ^{–1})	<i>L</i> _{FIR} (10 ¹³ L _⊙)	<i>M</i> _{bh} (10 ⁹ M _⊙)	\dot{M} _{acc} (M _⊙ yr ^{–1})
(1)	(2)	(3)	(4)	(5)	(6)	(7)	(8)	(9)	(10)	(11)
SDSS J1048+4637	6.23	–28.15	<3.4	–	0.94	<4.6	<50	<0.9	6.0	130
SDSS J1148+5251	6.43	–28.42	1.6 ^{1.9} _{1.3}	3.2 ^{4.5} _{2.0}	0.90	5.3	60	1.1	7.7	170
SDSS J1630+4012	6.05	–26.71	–	–	0.97	<4.5	<45	<0.9	1.6	35
Mean quasar	6.24	–27.76	2.13	1.65	0.94	–	–	–	4.2	90

Robson et al. (2004, MNRAS, 351, L29)

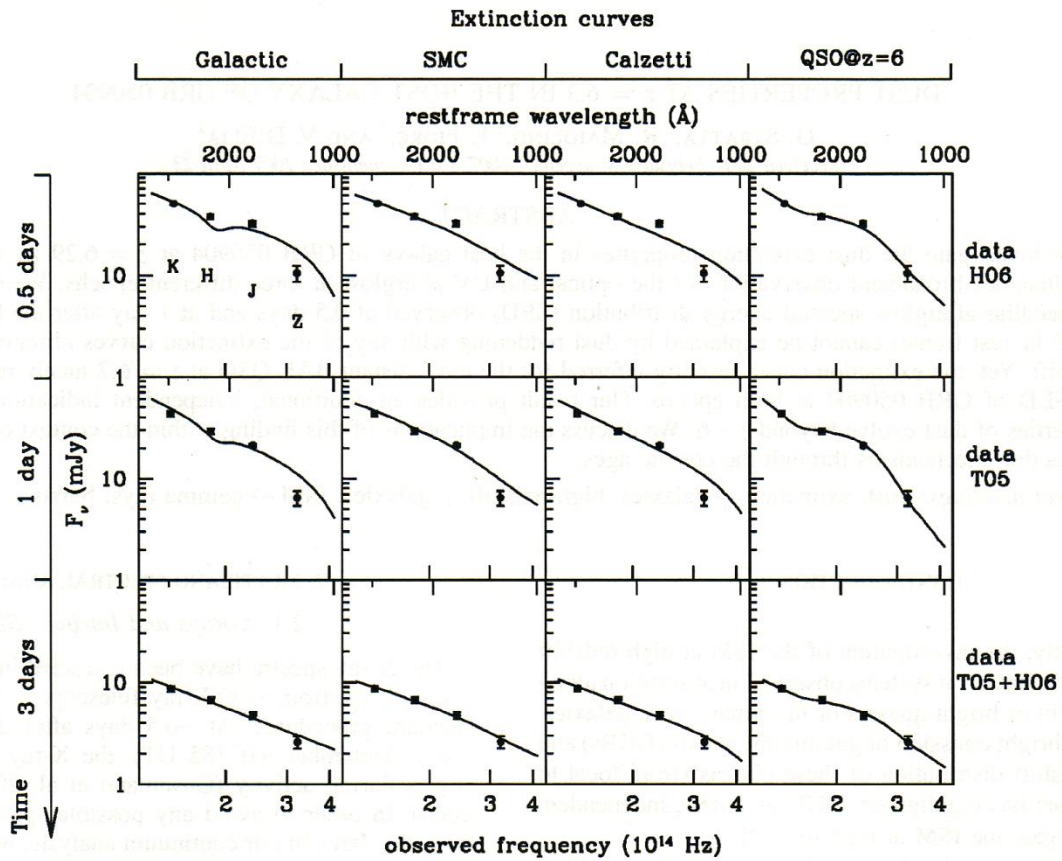
5-5. Extinction in high-z BAL quasars



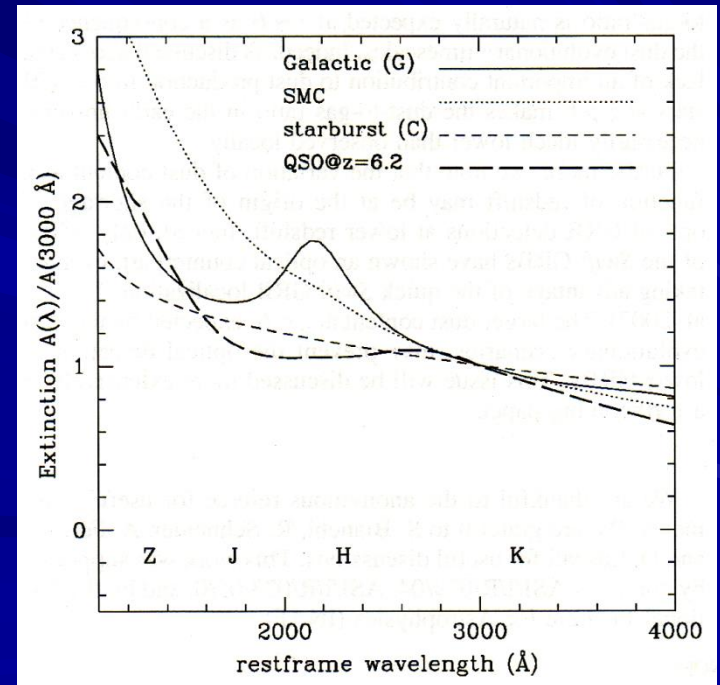
Maiolino et al.
(2004, A&A, 420, 889)

Source	z	$t(\infty) - t(z)$ Gyr	M_d $10^8 M_\odot$	\dot{M}_* (min) $M_\odot \text{ yr}^{-1}$	L_{FIR} $10^{10} L_\odot$	M_{bh} $10^9 M_\odot$	\dot{M}_{acc} $M_\odot \text{ yr}^{-1}$
SDSS J1306+0356	5.99	0.99 (0.70)	2.6 (1.8)	26	520 (370)	4.4 (3.0)	95 (65)
SDSS J1044-0125	5.74	1.04 (0.74)	4.2 (3.0)	41	870 (610)	5.6 (4.0)	125 (85)
SDSS J0756+4104	5.09	1.21 (0.86)	9.6 (6.9)	80	1970 (1410)	2.1 (1.4)	45 (30)
SDSS J0338+0021	5.07	1.22 (0.87)	8.5 (6.1)	70	1750 (1250)	2.1 (1.4)	45 (30)
SDSS J1030+0524	6.28	0.93 (0.66)	<1.4 (1.0)	–	<280 (200)	4.4 (3.0)	95 (65)
SDSS J0836+0054	5.82	1.02 (0.73)	<2.1 (1.5)	–	<430 (300)	7.6 (5.2)	165 (115)
RD J0301+0020	5.50	1.10 (0.78)	1.4 (1.0)	13	290 (200)	0.06 (0.04)	1.4 (0.9)
SDSS J2216+0013	4.99	1.25 (0.89)	<2.0 (1.4)	–	<410 (300)	1.9 (1.4)	40 (30)

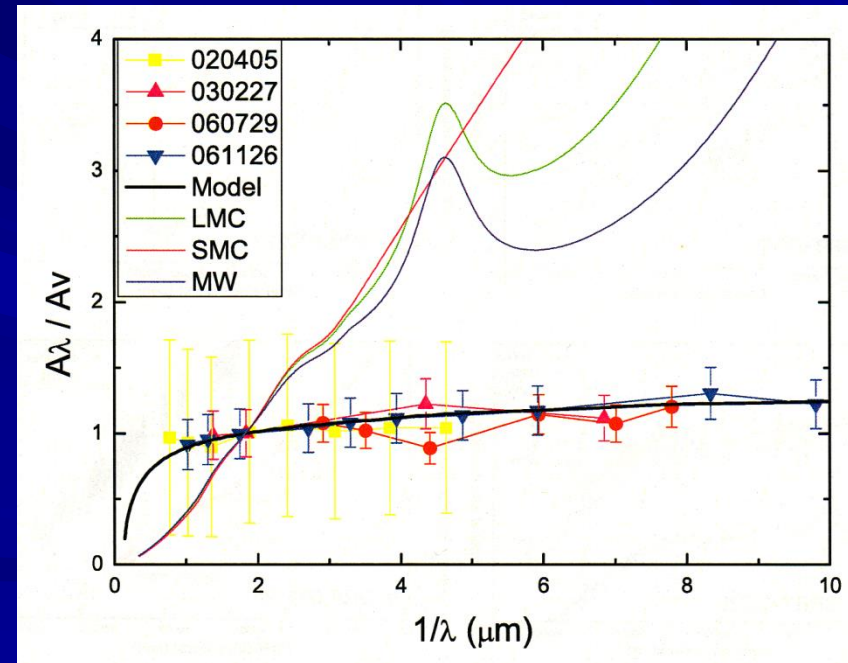
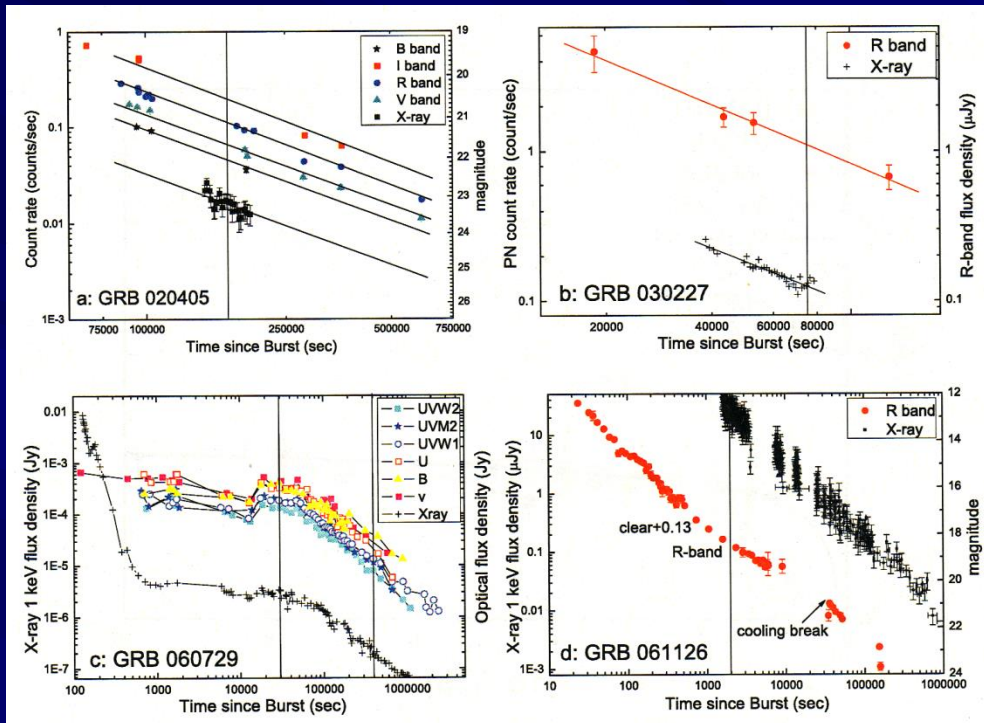
5-6. Extinction curves from GRBs



GRB 050904 at z=6.3
 Stratta et al. (2007, ApJ, 661, L9)



5-7. Extinction curves from GRBs



Li et al. (2008, astro-ph/0712.2622)

5-8. Extinction curves of AGNs

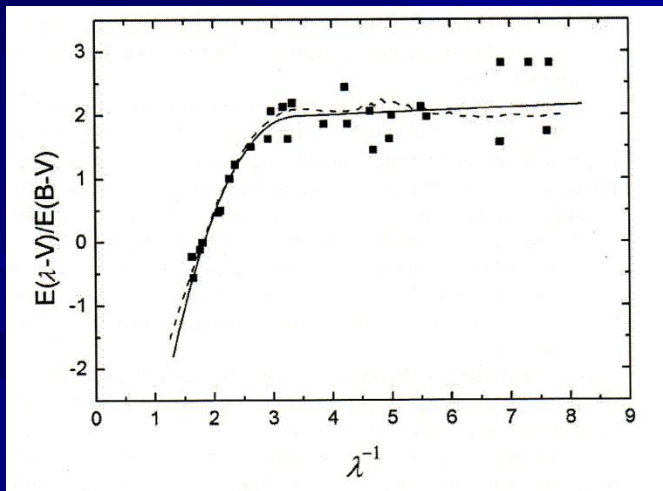
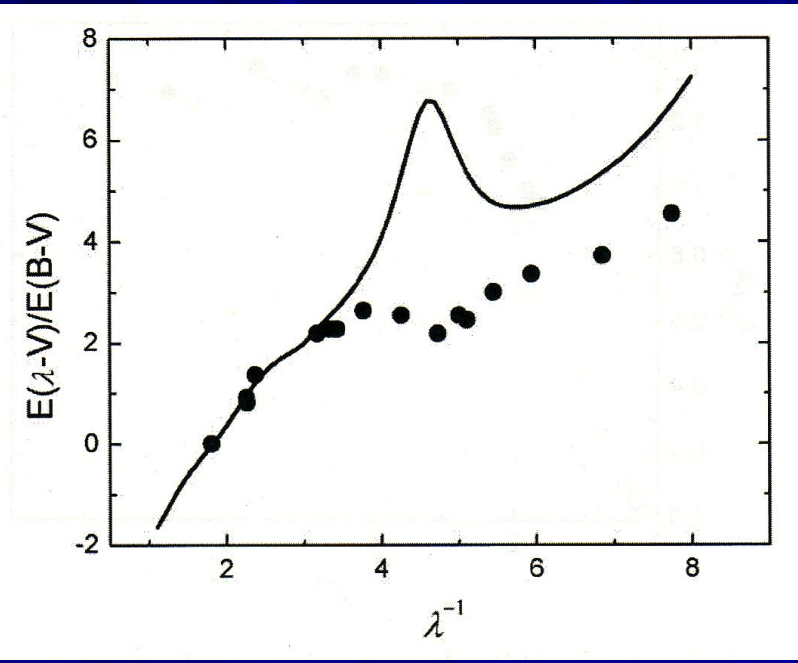
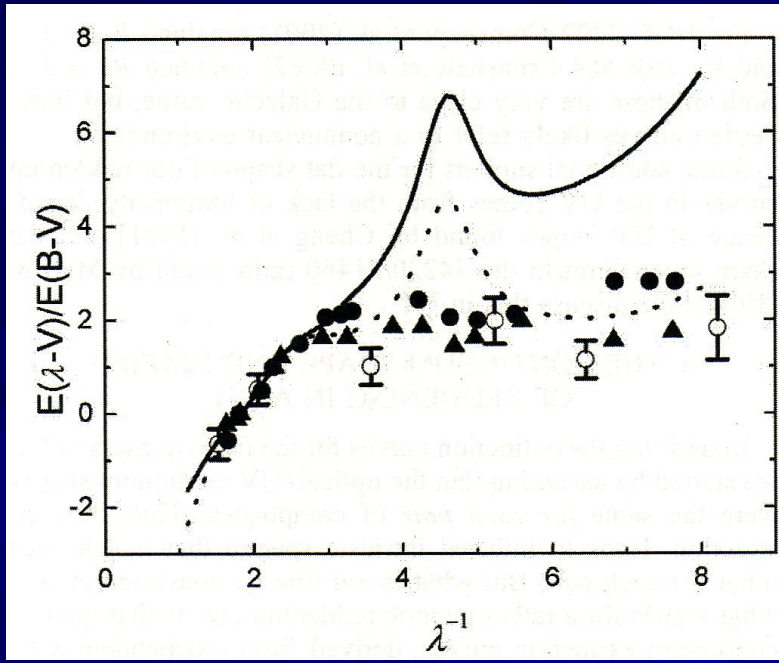
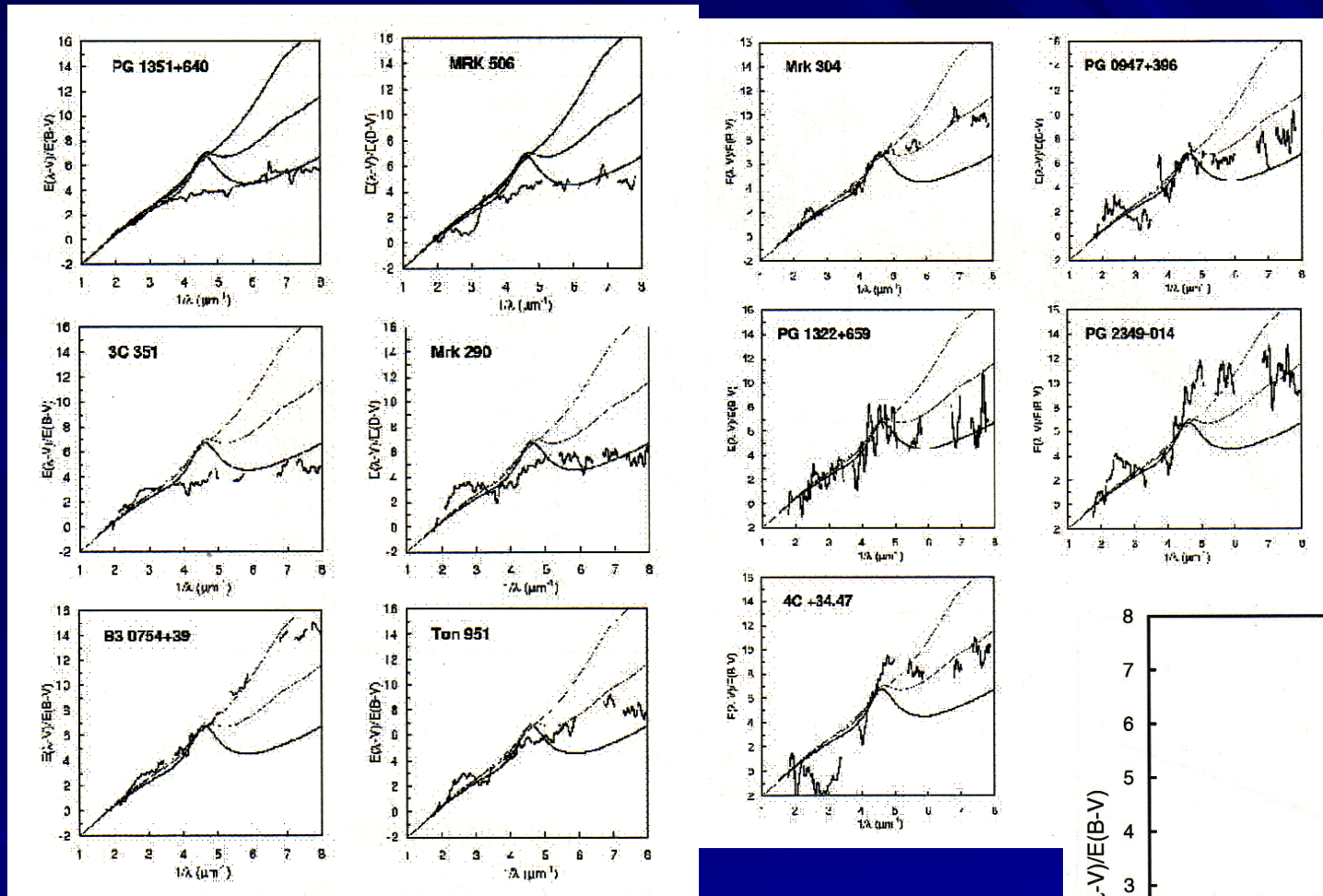


FIG. 6.—AGN extinction curves (*squares*) plotted together with a model curve derived from Mie theory computations (*dotted line*; see § 6.2) and the analytical fit given in the Appendix (*solid line*). Units are as in Fig. 1.

Gaskell et al. (2004, ApJ, 616, 147)

5-9. Extinction curves of AGNs



Gaskell & Benker (2008, astro-ph/0711.1013)

